In Silico Screening of Philippine Fabaceae-Derived Phenolic Acids as Potential NAGZ (B-Hexosaminidase) Inhibitors of Neisseria Gonorrhoeae (PDB ID: 6JTJ)

Grazel Ann M. Caspillo[1], Sittie Almiraiza A. Masukat[2], Cristylou Hearth P. Paladin[3], Daniella Dennise M. Po[4], Cynthia Claire F. Guinto[5], Erwin M. Faller[6]

Pharmacy Department, St. Alexius College, Inc. Philippines

DOI: https://doi.org/10.51244/IJRSI.2026.1306000167

Received: 31 May 2026; Accepted: 05 June 2026; Published: 29 June 2026

ABSTRACT

Neisseria gonorrhoeae remains a leading sexually transmitted pathogen worldwide and poses a public health challenge due to rising antimicrobial resistance. This crisis underscores the need for alternative treatment options. In this study, phenolic acids from Philippine Fabaceae plants were evaluated as potential inhibitors of the NagZ protein, an enzyme essential for bacterial cell wall recycling and survival. A total of 388 Fabaceae species obtained from Co's Digital Flora of the Philippines were screened based on reported phenolic acid content from existing journals and literature. Among these, 92 species were identified to contain documented phenolic acids, yielding a total of 37 distinct phenolic acids. In silico analyses included molecular docking, drug-likeness, ADMET profiling, and molecular dynamics simulations. Among the candidates, ellagic acid, 3,4-di-Ocaffeoylquinic acid, and 4-caffeoylquinic acid showed the strongest binding and favorable pharmacokinetic properties. These top-performing ligands were derived from: 3,4-di-O-caffeoylquinic acid was identified from the leaf of Cassia fistula, while 4-caffeoylquinic acid was obtained from the leaves of Medicago polymorpha. Ellagic acid was remarkably prevalent, found in the flowers of Caesalpinia pulcherrima, the pods of Parkia speciosa, and more. These findings highlight their potential as lead compounds, supporting further in vitro and in vivo validation against resistant gonorrhea.

Keywords: Neisseria Gonorrhoeae; NagZ (β-hexosaminidase); Phenolic acids; Fabaceae; In-silico; Molecular docking; ADMET; Drug-likeness; Molecular Dynamic Simulation

INTRODUCTION

Gonorrhea is a sexually transmitted disease (STD) caused by the obligate human pathogen Neisseria gonorrhoeae. It remains one of the most common sexually transmitted infections (STIs) both in the Philippines and globally. In 2020, the World Health Organization (WHO) estimated that approximately 82.4 million cases of gonorrhea occurred worldwide (Programmes, 2021).

At the national level, surveillance data indicate a rising number of STI cases. In Quezon City, a recent article reported 56% increase in the number of STI cases observed from 2021 to 2022, with gonorrhea accounting for the highest number of reported infections (Moaje, 2022). Locally, data from the Department of Health (DOH) shows that, from January 2020 to October 2025, the Provincial Epidemiology and Surveillance Unit recorded a total of 3,433 confirmed gonorrhea cases in the SOCCKSARGEN region, consist of 1,881 cases reported by Rural Health Units (RHUs) and 1,552 cases documented in hospital settings (DOH, 2025). This increasing trend over a five-year period highlights the high local prevalence of the disease and its growing impact on regional healthcare services and the need for effective control strategies.

Despite being preventable and treatable, N. gonorrhoeae poses ongoing challenges due to its ability to rapidly acquire antimicrobial resistance. As a result, it has been designated as a WHO Priority 2 pathogen for research and antibiotic development (Golparian & Unemo, 2022; Sarenie et al., 2022). Targeting alternative bacterial mechanisms is a promising approach to overcoming drug resistance (Murugaiyan et al., 2022). According to

Bhoophalan et al., (2016, as cited in Asma et al., 2022) found that one bacterial component implicated in resistance development of N. gonorrhoeae is the enzyme NagZ (β-Hexosaminidase). Previous studies have proposed that inhibiting the activity of NagZ may increase bacterial susceptibility to antibiotics (Yang et al., 2024). For this reason, NagZ is considered a promising molecular target for novel therapeutic strategies.

With the increasing demand for new therapeutic candidates, in silico methodologies have become widely utilized in early-stage drug discovery. These methods reduce the cost, time, and resources required in experimental research while supporting the rational identification of promising bioactive molecules (Brunner, 2023). Given the pathogen's complex physiology and the rapid emergence of resistance, researchers have turned their attention to plant-derived substances (AlSheikh et al., 2020). Among natural product sources, phenolic acids—a subclass of non-flavonoid polyphenols—have attracted scientific interest due to their antimicrobial, anti-inflammatory, and antioxidant properties (Liu, 2020). The Fabaceae family, which is abundant and well-represented in Philippine ecosystems, contains numerous species reported to produce phenolic acids associated with various biological activities (Obistioiu et al., 2021). Despite this, certain species within the family remain underexplored for their potential anti-gonococcal properties.

Although some plant-derived phenolic compounds have been studied for their antimicrobial activity against N. gonorrhoeae, there remains a lack of specific data on phenolic acids from Philippine Fabaceae species screened against NagZ (Yakobi et al., 2024). Thus, this study aims to perform an in silico screening of these compounds as potential inhibitors of the NagZ enzyme in N. gonorrhoeae, contributing to the development of new strategies to combat gonorrhea.

MATERIALS AND METHODS

Ligands and proteins preparation

Thirty-seven phenolic compounds derived from Philippine Fabaceae species were selected as candidate ligands for the present in silico investigation. These phytochemicals were identified from published literature based on their previously reported antimicrobial and therapeutic properties. The three-dimensional (3D) chemical structures and canonical SMILES of the selected ligands were retrieved from the PubChem database (https://pubchem.ncbi.nlm.nih.gov/) in Structure Data File (SDF) format.

The ligand structures were imported into PyRx version 0.8 for preprocessing and energy minimization. Optimization of ligand geometry was performed using the Universal Force Field (UFF) integrated with the Conjugate Gradient algorithm, employing 1000 iterations and an energy convergence criterion of 0.1 kcal/mol per step. Following minimization, all ligands were converted into PDBQT format using Open Babel embedded within the PyRx platform. Rotatable bonds were assigned to permit ligand flexibility during docking simulations (Dallakyan & Olson, 2015; Wojciechowski, 2017).

The crystal structure of the β-hexosaminidase enzyme (NagZ) of Neisseria gonorrhoeae (PDB ID: 6JTJ) was obtained from the RCSB Protein Data Bank (https://www.rcsb.org/) in Protein Data Bank (PDB) format. The receptor structure was prepared using AutoDock Tools by removing water molecules, heteroatoms, and co-crystallized ligands to eliminate unwanted interactions during docking analysis. Polar hydrogens and Kollman charges were subsequently added to optimize receptor geometry and electrostatic interactions prior to molecular docking.

Docking validation

To validate the reliability of the docking protocol, the native co-crystallized ligand was extracted from the receptor complex and re-docked into the active site using the same docking parameters and grid coordinates applied during molecular docking simulations. The inhibitor coordinates were isolated by manually removing non-receptor atoms from the crystal structure using Notepad++ and saving the extracted ligand separately in PDB format.

The re-docked ligand–protein complex was superimposed onto the original co-crystallized complex using

ISSN No. 2321-2705 | DOI: 10.51244/IJRSI |Volume XIII Issue VI June 2026

PyMOL version 2.3 to evaluate the accuracy of the reproduced binding pose. Root-mean-square deviation (RMSD) values were calculated to determine the similarity between the native and re-docked conformations. Ligand–protein interactions were further analyzed using LigPlot+ version 2.2.8 to assess the consistency of hydrogen bonding and hydrophobic interactions within the active site (C et al., 2022).

An RMSD value below the generally accepted threshold of 2.0 Å was considered indicative of a valid and reliable docking protocol capable of reproducing the experimentally observed binding orientation.

Molecular docking

Molecular docking simulations were carried out using PyRx version 0.8 employing the AutoDock Vina docking algorithm. The prepared receptor and ligand structures were converted into PDBQT format with the addition of polar hydrogens and atomic charges to facilitate docking calculations.

Docking simulations were performed using an exhaustiveness value of 20 to ensure extensive conformational sampling and accurate prediction of ligand binding poses. The docking grid box was centered on the active site coordinates corresponding to the position of the native co-crystallized ligand. Ligands were treated as flexible molecules, whereas the receptor protein remained rigid throughout the docking procedure (Ercan & Şenses, 2020; Sadhukhan et al., 2025; Shivanika et al., 2020)

Binding affinities were expressed in kilocalories per mole (kcal/mol), where more negative docking scores indicated stronger predicted ligand–protein interactions. To improve reproducibility and minimize stochastic variation associated with docking algorithms, each ligand was docked independently in five separate trials using identical docking parameters. Mean binding affinity values and standard deviations (mean ± SD) were subsequently calculated to evaluate the consistency and stability of docking results.

Table 1. Protein Information

Name	PDB ID	Crystallized Ligand	Organism	Classification	Method	Reference
NagZ	6JTJ	N-acetylglucosamine (NAG)	Neisseria gonorrhoeae	Hydrolase	X-ray Diffraction 2.18 Å	Chen, Y. Crystal structure of NagZ from Neisseria gonorrhoeae in complex with N-acetylglucosamine. RCSB Protein Data Bank. (rcsb.org)

Validation of Binding Affinity Results

To ensure reproducibility and minimize stochastic variation associated with molecular docking algorithms, docking simulations for each ligand were independently performed five times using identical docking parameters. Binding affinity values obtained from the five docking trials were analyzed using descriptive statistics, specifically mean and standard deviation (mean ± SD).

The mean binding affinity represented the overall predicted interaction strength of each ligand with the NagZ receptor, whereas the standard deviation reflected the consistency and variability of the docking results. Ligands exhibiting highly negative mean binding affinity values accompanied by low standard deviation were interpreted as possessing stronger and more stable predicted interactions with the target protein. Performing multiple docking runs minimized the influence of random variations inherent in stochastic search algorithms and reduced bias from a single docking output, thereby enhancing the reliability and consistency of the predicted ligand–protein interactions.

In Silico Pharmacokinetics and Drug-Likeness Evaluation

The top-performing phytochemicals identified from molecular docking analysis were further subjected to in silico ADMET and drug-likeness evaluation to assess their pharmacokinetic suitability and toxicological profiles. Canonical SMILES representations of the compounds were analyzed using several online

ISSN No. 2321-2705 | DOI: 10.51244/IJRSI |Volume XIII Issue VI June 2026

computational platforms, including SwissADME (http://www.swissadme.ch/), ADMETLab 2.0 (https://admetmesh.scbdd.com/), pkCSM (https://biosig.lab.uq.edu.au/pkcsm/), and ProTox-III (https://tox.charite.de/protox3/).

Drug-likeness parameters such as molecular weight, partition coefficient (logP), topological polar surface area (TPSA), hydrogen bond donors and acceptors, and rotatable bond count were evaluated according to Lipinski's Rule of Five and Veber's Rule to determine oral bioavailability potential (Daina et al., 2017).

Additional pharmacokinetic properties including aqueous solubility, Caco-2 permeability, intestinal absorption, skin permeability, blood–brain barrier permeability, cytochrome P450 enzyme interactions, renal excretion, and total clearance were predicted using pkCSM (Azzam, 2023). Toxicological parameters such as acute oral toxicity (LD_{50}), toxicity class, hepatotoxicity, mutagenicity, carcinogenicity, cytotoxicity, and immunotoxicity were predicted using ProTox-III (Fekadu et al., 2022). All analyses were performed using default computational parameters to ensure reproducibility across software platforms.

Table 2. Grid center and dimension of protein

PDB ID	Vina Search Space					
	Center			Dimensions (Å)		
	X	Y	Z	X	Y	Z
6JTJ	35.2406	84.3793	102.5149	25	25	25

Molecular Dynamic Simulation

To further evaluate the structural stability and conformational dynamics of the docked complexes beyond static docking predictions, molecular dynamic (MD) simulations were performed using GROMACS version 2025.1. Only the top three ligand–protein complexes, selected based on mean binding affinity values obtained from molecular docking, were subjected to MD simulation due to the computational intensity of the procedure. Protein parameterization was conducted using the CHARMM36 force field, while ligand topologies were generated through SwissParam (https://www.swissparam.ch/) (K & Venugopal, 2024). Protonation states were assigned at physiological pH (7.4) using PDB2PQR (https://server.poissonboltzmann.org/pdb2pqr). Each complex was solvated in a cubic simulation box maintaining a 10 Å distance between the solute and box edges using the CHARMM-TIP3P water model. Sodium (Na^+) and chloride (Cl^-) ions were added to neutralize the system and establish an ionic concentration of 0.15 M.

Energy minimization was carried out using the steepest-descent algorithm until the maximum force decreased below 1000 $kJ \cdot mol^{-1} \cdot nm^{-1}$. System equilibration involved a 500 ps NVT ensemble at 300 K using the velocity-rescale thermostat, followed by a 500 ps NPT ensemble at 1 bar pressure employing the Parrinello–Rahman barostat (Ke et al., 2022) Production simulations were conducted for 100 ns with a 2-fs integration time step, and trajectory frames were saved every 100 ps. Long-range electrostatic interactions were treated using the Particle Mesh Ewald (PME) method with a 1.2 nm cutoff for short-range interactions (Abraham et al., 2015; Páll et al., 2020).

Structural stability and conformational dynamics of the complexes were analyzed through root-mean-square deviation (RMSD), root-mean-square fluctuation (RMSF), radius of gyration (Rg), solvent-accessible surface area (SASA), and hydrogen bond occupancy using standard GROMACS analysis tools (Purohit, 2014; Rajendran et al., 2018; Sharma et al., 2021; Singh et al., 2021). Binding free energies of the equilibrated complexes were further estimated using the Molecular Mechanics/Generalized Born Surface Area (MM/GBSA) approach implemented in gmx_MMPBSA version 1.6.3 (Valdés-Tresanco et al., 2021).

RESULTS AND DISCUSSION

Molecular Docking Results

The molecular docking results showed binding energies ranging from −5.70 to −9.70 kcal/mol, where more

ISSN No. 2321-2705 | DOI: 10.51244/IJRSI |Volume XIII Issue VI June 2026

negative values indicate stronger and more favorable ligand–protein interactions due to increased thermodynamic stability (Pinzi & Rastelli, 2019). Among the evaluated ligands, ellagic acid demonstrated the strongest binding affinity (−9.70 kcal/mol), followed by 3,4-di-O-caffeoylquinic acid and 4-caffeoylquinic acid (−8.80 kcal/mol). These polyphenolic compounds contain multiple hydroxyl groups and extended aromatic structures (Magaña et al., 2021), which may enhance hydrogen bonding, hydrophobic interactions, and electrostatic forces within protein binding pockets (Baruah et al., 2022). Hydrogen bonding plays a key role in ligand binding affinity and selectivity (Madushanka et al., 2023), explaining the stronger interactions observed among structurally complex polyphenols compared with simpler phenolic compounds (Bano & Malik, 2022). The identified ligands are also present in medicinal plants such as Cassia fistula, Cassia grandis, Caesalpinia pulcherrima, Clitoria ternatea, and Medicago polymorpha, supporting their pharmacological relevance. Furthermore, Gutiérrez-Durán et al. (2026) reported that flavonoids, alkaloids, and particularly phenolic compounds exhibit notable antimicrobial activity, while Mongalo and Raletsena (2023) identified the genus Cassia as widely used in traditional medicine for sexually transmitted infections. Collectively, these findings support the potential of Fabaceae-derived phytochemicals as promising lead compounds against Neisseria gonorrhoeae.

Table 3. Molecular Docking Results of lead ligands

Binding Energy							**Average**
Ligands		Trial 1	Trial 2	Trial 3	Trial 4	Trial 5	
1	Ellagic acid	-9.7	-9.7	-9.7	-9.7	-9.7	-9.70
2	3,4-di-O-caffeoylquinic acid	-8.7	-9.6	-9.1	-9.5	-9.6	-9.30
3	4-Caffeoylquinic acid	-8.8	-8.8	-8.8	-8.8	-8.8	-8.80

Docking Validation

The reliability of the docking protocol was confirmed through successful redocking of the native ligand into the active site of PDB ID: 6JTJ. As illustrated in Figure 1, the superimposition of the re-docked and co-crystallized ligand showed good spatial agreement. The 6JTJ complex exhibited an RMSD value of 1.82 Å, which falls within the acceptable threshold (≤ 2.0 Å), indicating that the docking protocol was able to satisfactorily reproduce the native binding pose. Interaction analysis using LigPlot+ (Figure 2) further supported these findings, where interacting residues were found to overlap with those of the native ligand, indicating conservation of key binding interactions within the active site.

Overall, these results demonstrate that the docking protocol is reliable and capable of reproducing experimentally observed binding modes.

Figure 1. Superimposition of re-docked (blue) and native (red) ligands in PDB ID: 6JTJ (RMSD = 1.82 Å), visualized in PyMOL.

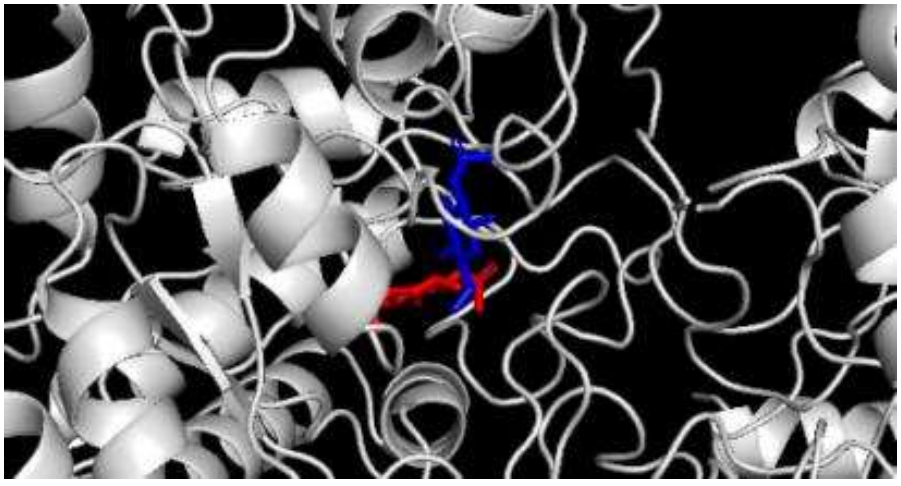

ISSN No. 2321-2705 | DOI: 10.51244/IJRSI |Volume XIII Issue VI June 2026

Drug-likeness Properties

The table summarizes the physicochemical and drug-likeness properties of the top ligands predicted using ADMETLab 2.0. Thirty-six of the 37 evaluated phenolic acids satisfied Lipinski's Rule of Five, indicating generally favorable drug-like characteristics. Only 3,4-di-O-caffeoylquinic acid violated the rule due to its relatively high molecular weight (516.45 g/mol) and high numbers of hydrogen bond donors and acceptors, which may reduce membrane permeability and oral bioavailability.

In contrast, all top three ligands—3,4-di-O-caffeoylquinic acid, 4-caffeoylquinic acid, and ellagic acid—failed Veber's Rule because of elevated topological polar surface area (TPSA) values exceeding 140 Å². High TPSA is commonly associated with reduced passive membrane permeability; however, all three ligands satisfied the rotatable bond criterion, indicating acceptable molecular flexibility (Cornelissen et al., 2023). Although elevated polarity may limit oral absorption, it also enhances the ability of phenolic compounds to form strong intermolecular interactions with biological targets (Vidal de Barros Rêgo, 2026).

The top ligands are widely distributed among medicinal plants rich in polyphenolic constituents, including Cassia fistula, Medicago polymorpha, Caesalpinia pulcherrima, and Clitoria ternatea. Previous studies have associated these phytochemicals with favorable biological activities and molecular recognition properties (Gutiérrez-Durán et al., 2026). Despite deviations from Veber's criteria, the strong binding affinities and acceptable Lipinski profiles of the top ligands support their potential as promising candidates for further drug development and optimization (Tariq et al., 2024).

Table 4. Drug-likeness properties of lead ligands

Compounds		MW (gm/mol)	NRB	NHA	NHD	TPSA (Å²)	LogP (clogP)	Lipinski's rule violation	Veber's rule violation
1	**Ellagic acid**	302.010	0	8	4	141.340	1.117	Accepted	Rejected
2	**3,4-di-O-caffeoylquinic acid**	516.45	9	12	7	211.28	3,4-di-O-caffeoylquinic acid	516.45	9
3	**4-Caffeoylquinic acid**	354.31	5	9	6	164.75	-0.37	Accepted	Rejected

Pharmacokinetic Properties

The pharmacokinetic properties of the identified phytochemicals were evaluated using the pkCSM platform, as summarized in Table 4. The predicted absorption parameters showed variability among the phenolic acids, particularly for caffeoylquinic acid derivatives, which demonstrated low human intestinal absorption values, likely due to limited passive membrane permeability associated with their high polarity. In contrast, ellagic acid exhibited relatively high predicted intestinal absorption, suggesting more favorable oral uptake.

Distribution parameters indicated generally moderate systemic distribution, while most compounds demonstrated poor blood–brain barrier permeability, suggesting limited central nervous system penetration. Metabolic predictions showed minimal cytochrome P450 inhibition, and none of the top ligands were predicted to inhibit major CYP isoforms or act as OCT2 substrates, indicating a favorable metabolic safety profile (Clifford et al., 2020). Additionally, caffeoylquinic acid derivatives demonstrated relatively lower clearance values, suggesting prolonged systemic residence time.

The ADME profiles of the top ligands suggest that, despite potential limitations in passive absorption, they possess favorable metabolic and excretory characteristics. Recent studies have further demonstrated that formulation strategies such as nanoencapsulation, liposomal delivery, and phytosome systems may improve the bioavailability and permeability of phenolic compounds (Cosme et al., 2020; Grgić et al., 2020). Collectively, these findings support the continued investigation of these plant-derived phenolic acids as promising candidates for antibacterial drug development (Mandal et al., 2024).

ISSN No. 2321-2705 | DOI: 10.51244/IJRSI |Volume XIII Issue VI June 2026

Table 5. Pharmacokinetic properties of lead ligands

COMPOUNDS		ABSORPTION				DISTRIBUTION				METABOLISM	EXCRETION	
		Water solubility (log mol/L)	Caco2 Permeability (log Papp in 10-6 cm/s)	HIA (% Absorbed)	Skin Permeability (log Kp)	VDss (human) (log L/kg)	Fraction unbound (human) (Fu)	BBB permeability (log BB)	CNS permeability (log PS)	CYP2D6 substrate CYP3A4 substrate CYP1A2 inhibitor CYP2C19 inhibitor CYP2C9 inhibitor	Total Clearance (log ml/min/kg)	Renal OCT2 substrate
1	**Ellagic acid**	-3.181	0.335	86.684	-2.735	0.375	0.083	-1.272	-3.533	No; No; Yes; No; No	0.537	No
2	**3,4-di-O-caffeoylquinic acid**	-2.955	-1.203	29.037	-2.735	-2.735	0.294	-2.08	-3.804	No; Yes; No; No; No	-0.042	No
3	**4-Caffeoylquinic acid**	-2.428	-0.892	20.029	-2.735	0.546	0.662	-1.593	-3.791	No; No; No; No; No	0.298	No

Toxicity Characteristics

The predicted acute toxicity of the tested phenolic acids, expressed as LD_{50} values, indicates that most compounds fall within toxicity classes 4–6, corresponding to low to moderate toxicity levels. Glycosylated compounds such as 1-O-sinapoyl-β-D-glucose, 3,4-di-O-caffeoylquinic acid, and 4-caffeoylquinic acid exhibit high LD_{50} values (≥ 5000 mg/kg), placing them in toxicity class 5 and suggesting relatively low acute toxicity and a wider safety margin for potential therapeutic applications. In comparison, smaller non-glycosylated phenolic acids such as cinnamic acid, p-coumaric acid, and o-coumaric acid demonstrate slightly lower LD_{50} values (approximately 2500–2850 mg/kg), corresponding to moderate toxicity (class 5), yet still considered acceptable for oral administration in early drug development stages. Conversely, compounds such as methyl ferulate, salicylic acid, and gallic acid ethyl ester present LD_{50} values below 1200 mg/kg, placing them in toxicity class 4 and indicating comparatively higher acute toxicity. Variations in molecular structure, such as esterification or methoxy substitutions, can influence toxicity profiles among phenolic acids (Kiokias & Oreopoulou, 2021; Kiriyama et al., 2024).

Hepatotoxicity predictions reveal that most evaluated phenolic acids are classified as inactive; however, several compounds—including 4-methoxycinnamic acid, 5-methoxysalicylic acid, cinnamic acid, gallic acid ethyl ester, methyl ferulate, and salicylic acid—were predicted to exhibit hepatotoxic potential. Drug-induced liver injury is a common cause of drug withdrawal, highlighting the importance of early toxicity screening to identify compounds requiring further toxicological investigation (Chen et al., 2025). Carcinogenicity predictions were largely negative across the tested phenolic acids, although several compounds, including 3,4-dihydroxy-trans-cinnamic acid, caffeic acid, ellagic acid, gallic acid, m-coumaric acid, p-coumaric acid, p-coumaric acid-O-glucoside, methyl ferulate, and rosmarinic acid, were predicted to possess potential carcinogenic effects. Structural diversity among phenolic compounds may lead to different biological and toxicological responses, emphasizing the need for further long-term safety evaluation (Zhu et al., 2024). Mutagenicity, immunotoxicity, and cytotoxicity profiles are largely inactive across the phenolic acids, suggesting minimal genotoxic, immune-disruptive, or general cytotoxic risks. Active immunotoxicity was observed in 1-O-sinapoyl-beta-D-glucose and 3,4-di-O-caffeoylquinic acid.

Among the evaluated compounds, the top three with the highest binding affinity ligands—3,4-di-O-caffeoylquinic acid, 4-caffeoylquinic acid, and ellagic acid—demonstrate generally favorable acute toxicity profiles. Both 3,4-di-O-caffeoylquinic acid and 4-caffeoylquinic acid exhibit high predicted LD_{50} values of ≥ 5000 mg/kg, corresponding to low acute toxicity (class 5), while ellagic acid shows a moderately lower LD_{50} value of approximately 2850 mg/kg (class 5), indicating moderate toxicity but still within an acceptable range for oral administration. The absence of widespread mutagenic and cytotoxic predictions for all three ligands further supports their safety in terms of genotoxic and general cytotoxic risks; however, specific predicted

ISSN No. 2321-2705 | DOI: 10.51244/IJRSI |Volume XIII Issue VI June 2026

endpoints, including immunotoxicity for 3,4-di-O-caffeoylquinic acid and potential carcinogenicity for ellagic acid, underscore the importance of targeted in vitro and in vivo studies. Overall, the toxicity predictions support the use of computational toxicity profiling as an effective preliminary screening step for identifying safe phytochemical candidates in drug discovery (Banerjee et al., 2021).

Table 6. Toxicity Characteristics of lead ligands

Compounds		LD50 (mg/kg)	Toxic Class	Organ Toxicity				
				Hepatotoxicity	Carcinogenicity	Immunotoxicity	Mutagenicity	Cytotoxicity
1	**1-O-sinapoyl-beta-D-glucose**	5000mg/kg	5	Inactive	Inactive	Active	Inactive	Inactive
2	**3-Hydroxybenzoic acid**	2000mg/kg	4	Inactive	Inactive	Inactive	Inactive	Inactive
3	**3,4-di-O-caffeoylquinic acid**	5000mg/kg	5	Inactive	Inactive	Active	Inactive	Inactive

Interaction stability

Molecular docking analysis of ellagic acid, 3,4-di-O-caffeoylquinic acid, and 4-caffeoylquinic acid against protein 6JTJ revealed networks of non-covalent interactions, indicating varying levels of interaction stability. All ligands engaged in hydrogen bonding, hydrophobic interactions, and van der Waals contacts within the catalytic pocket. Among the compounds, 3,4-di-O-caffeoylquinic acid and 4-caffeoylquinic acid exhibited more extensive interaction patterns, forming multiple hydrogen bonds and hydrophobic contacts, suggesting favorable spatial orientation and energetic complementarity within the binding pocket. Hydrophobic interactions play a crucial role in providing thermodynamic stability to folded proteins (Baldwin et al., 2016, as cited in Ferenczy & Kellermayer, 2022). Ellagic acid and the caffeoylquinic acid derivatives maintained substantial hydrophobic and van der Waals interactions that contributed to overall complex stability, highlighting the importance of cooperative non-covalent forces in stabilizing polyphenolic ligands.

In structure-based drug design, docking stability is attributed to the cumulative effect of non-covalent interactions that lower binding free energy and restrict ligand mobility (Sahu et al., 2024). Studies emphasize that stable receptor–ligand complexes arise from a balance of hydrogen bonding, hydrophobic, electrostatic, and van der Waals interactions rather than hydrogen bonding alone (Mohanty et al., 2023). The extensive contact networks observed for 3,4-di-O-caffeoylquinic acid and 4-caffeoylquinic acid support their enhanced stability, while the strong binding affinity of ellagic acid may be attributed to its rigid polyphenolic framework enabling efficient hydrophobic packing and stable non-covalent contacts. Collectively, these findings support the potential of these ligands for further molecular dynamics simulations and experimental validation.

Figure 2. (a) 2D and 3D Structures of Ellagic acid–6JTJ complex, (b) 3,4-di-O-caffeoylquinic acid–6JTJ complex, (c) 4-caffeoylquinic acid/Cryptochlorogenic acid complex.

a)

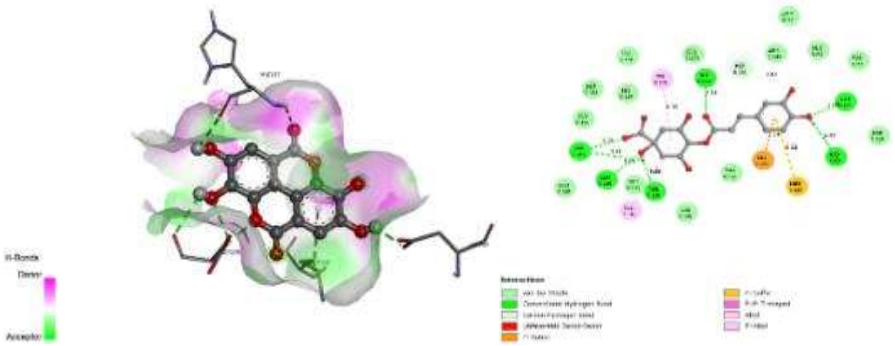

ISSN No. 2321-2705 | DOI: 10.51244/IJRSI |Volume XIII Issue VI June 2026

(b)

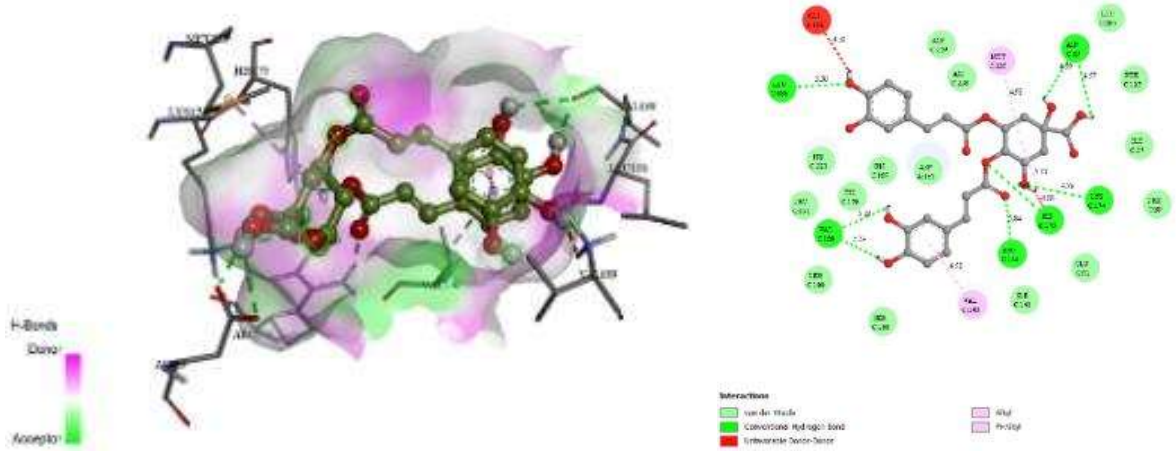

(c)

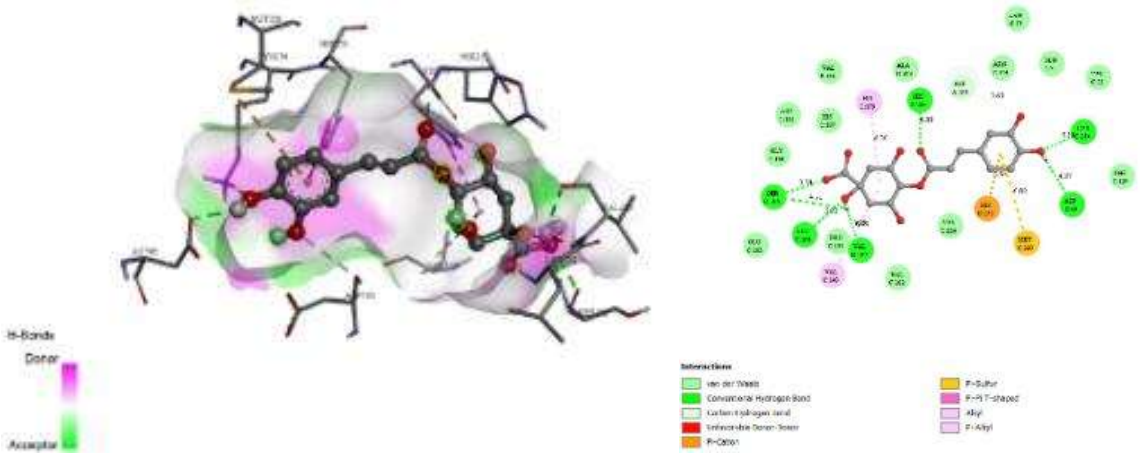

Hydrogen Bonding Patterns

Hydrogen bonds are critical components of protein–ligand complexes because they provide directional specificity and significant stabilization energy, anchoring the ligand within the binding site (Nivatya, 2025). In the present study, Ellagic acid formed key hydrogen bonds with HIS 187, ASP 69, and ASP 259. 3,4-di-O-caffeoylquinic acid established an extensive pattern of hydrogen bonding with multiple residues, whereas 4-Caffeoylquinic acid also formed several hydrogen bonds across the pocket. Recent literature supports the importance of hydrogen bonding as a core determinant in protein-ligand binding specificity and stability (Nivatya, 2025). Hydrogen bonds, as polar non-covalent interactions, lower the enthalpic component of binding free energy and are often correlated with improved binding affinity when complemented by hydrophobic interactions and other contact types (Sharif Ezzaz, 2024).

However, hydrogen bond counts alone are not sufficient predictors of binding affinity; rather, the quality, geometry, and persistence of hydrogen bonds combined with the broader interaction environment influence complex stability (Mohanty et al., 2023). Contemporary studies on docking interaction prediction show that modern interaction-aware models which directly capture hydrogen bond networks and hydrophobic contacts provide improved performance over approaches focusing solely on geometric fit (Lai et al., 2024). In sum, the

ISSN No. 2321-2705 | DOI: 10.51244/IJRSI |Volume XIII Issue VI June 2026

observed hydrogen bond networks—particularly those formed by 3,4-di-O-caffeoylquinic acid and 4-Caffeoylquinic acid—are likely to enhance the binding specificity and stability of these ligands in the active site of 6JTJ, supporting their prospects for further in-depth biochemical validation.

Table 7. Hydrogen bonding patterns of lead ligands

PDB ID	Ligands	H bond	Amino acid interactions	
			Hydrophobic/ Pi-cation/ Pi anion/ Pi-alkyl interaction/Pi-Sulfur/Unfavorable Donor-Donor	Van der Waals interaction
6JTJ	Ellagic acid	HIS 187, ASP 69, ASP 259	MET 220	VAL 140, HIS 179, SER 186, ASP 185, HIS 175, ARG 144, GLU 71, LYS 174, PHE 127, LEU 287, ASP 258, LEU 188, HIS 223
	3,4-di-O-caffeoylquinic acid	LEU 188, VAL 189, ARG 144, HIS 175, LYS 174, ASP 69	MET 220, VAL 140, VAL 189	LEU 287, PHE 127, ILE 37, PHE 39, GLU 71, ILE 141, SER 186, LEU 190, PRO 191, HIS 179, HIS 187, ASP 185, HIS 223, ASP 259, ASP 258
	4-Caffeoylquinic acid/cryptochlorogenic acid	LYS 174, ASP 69, VAL 189, LEU 188, SER 186, HIS 223, ASP 185	HIS 179, VAL 140, HIS 175, MET 220	ARG 77, GLU 71, VAL 75, ARG 144, PHE 127, VAL 224, VAL 182, PRO 191, GLU 183, GLY 184, ASP 185, HIS 187, VAL 140, ALA 222

Receptor–Ligand Complementarity Within the Catalytic Pocket

Visual inspection of the docking poses reveals that all three ligands—Ellagic acid, 3,4-di-O-caffeoylquinic acid, and 4-Caffeoylquinic acid (cryptochlorogenic acid)—fit snugly within the catalytic pocket of 6JTJ, demonstrating high steric and chemical complementarity. Ellagic acid aligns centrally within the binding cavity, with its planar aromatic rings nestled between hydrophobic residues and forming hydrogen bonds with HIS 187, ASP 69, and ASP 259 (Figure A). 3,4-di-O-caffeoylquinic acid occupies a larger portion of the cavity, allowing multiple polar interactions across the pocket. Hydrogen bonds with LEU 188, VAL 189, ARG 144, HIS 175, LYS 174, and ASP 69 anchor the ligand, while hydrophobic contacts with MET 220, VAL 140, and VAL 189 further stabilize the complex (Figure B). 4-Caffeoylquinic acid spans the pocket in a similar orientation, forming hydrogen bonds with LYS 174, ASP 69, VAL 189, LEU 188, SER 186, HIS 223, and ASP 185, while simultaneously engaging hydrophobic residues such as VAL 140 and MET 220 (Figure C).

Overall, the docking poses indicate that all three phenolic compounds demonstrate excellent receptor–ligand complementarity, combining proper steric fit with favorable electrostatic and hydrophobic interactions. This complementarity enhances ligand stabilization, binding specificity, and potential inhibitory activity, consistent with the principles of structure-based drug design (Lai et al., 2024; Mohanty et al., 2023). The extensive overlap of ligand surfaces with the catalytic pocket, along with complementary hydrogen bonding and hydrophobic interactions, suggests that these ligands are well-positioned to effectively occupy and inhibit the target site.

ISSN No. 2321-2705 | DOI: 10.51244/IJRSI |Volume XIII Issue VI June 2026

Figure 3. (a) Catalytic Pocket Complementarity of Ellagic acid–6JTJ complex, (b) 3,4-di-O-caffeoylquinic acid–6JTJ complex, (c) 4-caffeoylquinic acid/Cryptochlorogenic acid complex.

(a)

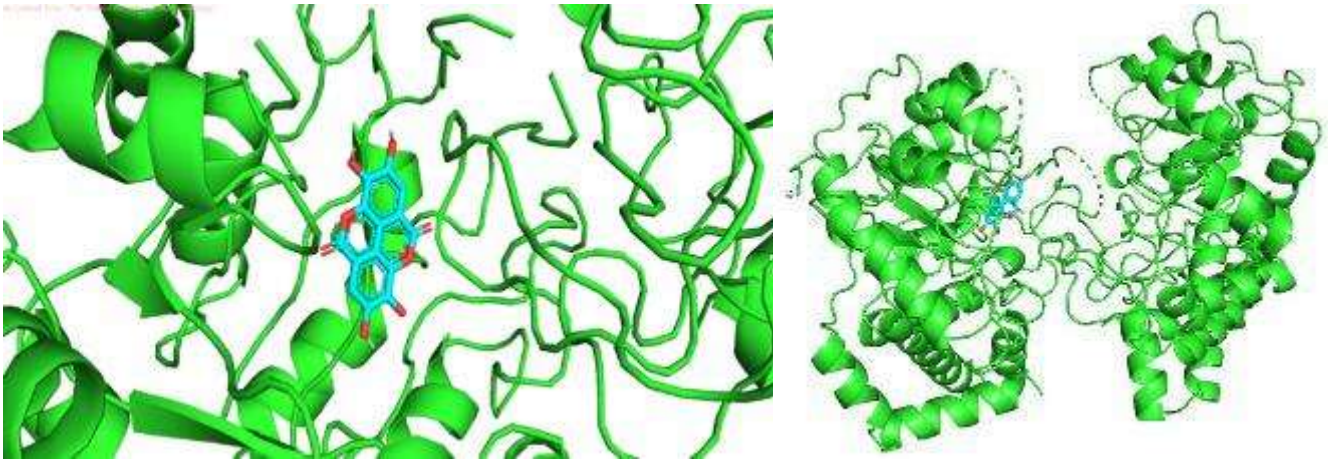

(b)

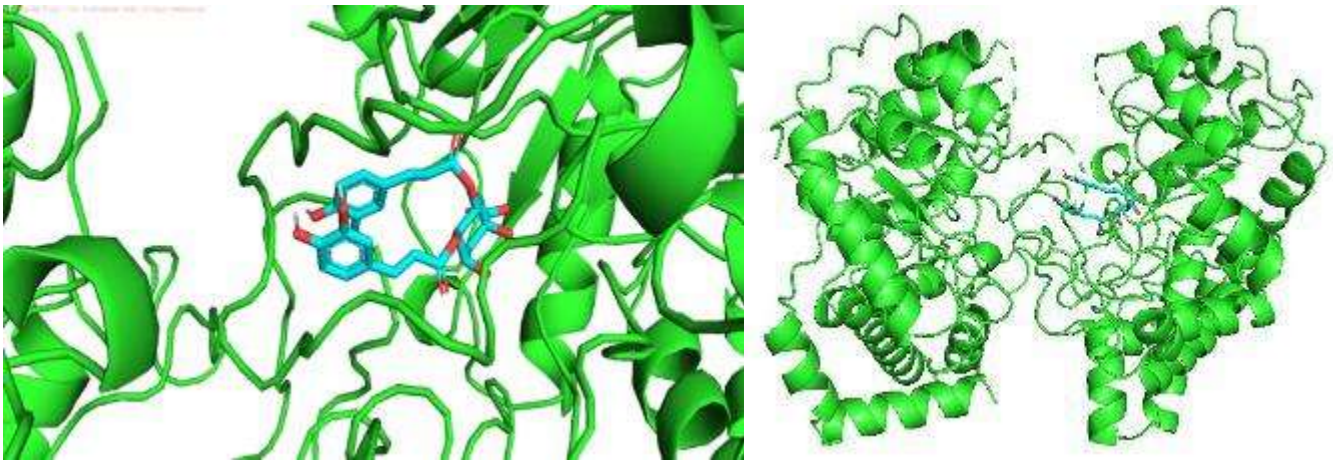

(c)

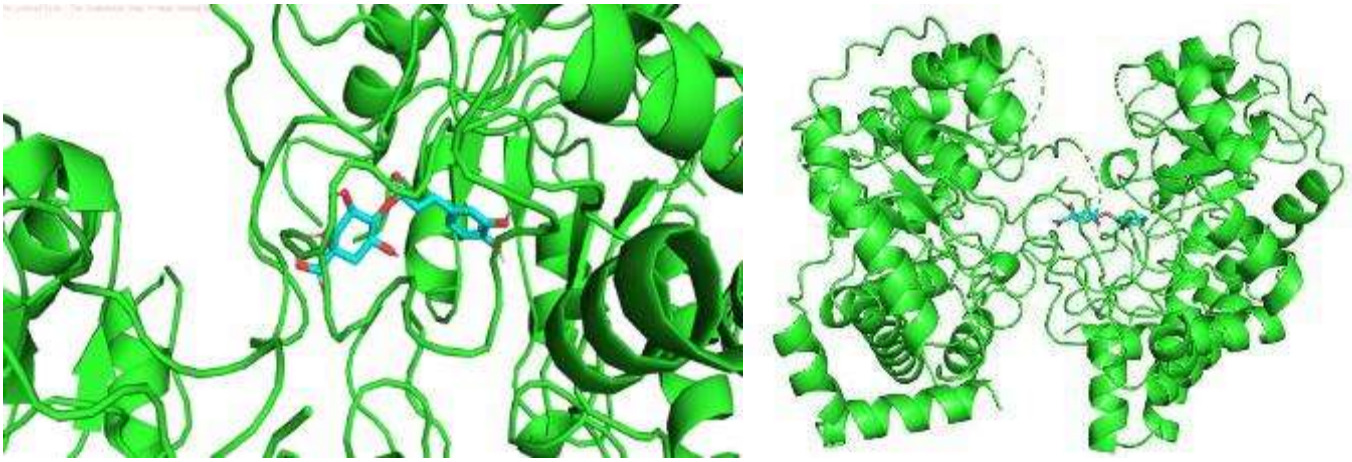

A. Root-Mean-Square Deviation (RMSD) Analysis

Root-mean-square deviation (RMSD) analysis was conducted to evaluate the structural stability of the three 6JTJ–ligand complexes during molecular dynamics simulation. Among the complexes, 6JTJ–3,4-di-O-caffeoylquinic acid (CID: 5281780) exhibited the highest average RMSD (0.162 ± 0.046 nm), with fluctuations ranging from 0.0005 to 0.316 nm, indicating greater conformational flexibility. A pronounced increase at

ISSN No. 2321-2705 | DOI: 10.51244/IJRSI |Volume XIII Issue VI June 2026

approximately 2.4 ns suggested an initial structural rearrangement associated with equilibration, a phenomenon commonly attributed to the adaptation of the protein–ligand complex from its docked state to a more energetically favorable conformation (Guterres & Im, 2020). Despite this early fluctuation, the absence of continuous RMSD escalation indicates that the system successfully attained equilibrium and maintained structural stability throughout the simulation. The 6JTJ–cryptochlorogenic acid complex (CID: 9798666) displayed a lower average RMSD of 0.114 ± 0.036 nm, with values ranging from 0.0005 to 0.213 nm, reflecting reduced structural deviation. Although a transient fluctuation was observed at approximately 48.3 ns, no progressive instability was detected, suggesting preserved conformational integrity.

In contrast, the 6JTJ–ellagic acid complex (CID: 5281855) demonstrated the lowest RMSD values, with an average of 0.030 ± 0.007 nm and a narrow fluctuation range of 0.0004–0.0704 nm, indicating highly restricted atomic displacement and exceptional structural stability. A minor deviation at approximately 38.3 ns was observed but was not followed by significant drift, suggesting stable retention of the ligand within the binding pocket. Consistent with the findings of Sasidharan et al. (2023), low and stable RMSD values are indicative of strong binding affinity and sustained protein–ligand interactions. Overall, the RMSD profiles revealed differential stability among the complexes, with ellagic acid demonstrating the highest structural stability, followed by cryptochlorogenic acid, while 3,4-di-O-caffeoylquinic acid showed comparatively greater flexibility but remained equilibrated, supporting its stable interaction with the target protein.

Figure 4. Backbone RMSD Profiles of the 6JTJ–Ligand Complexes.

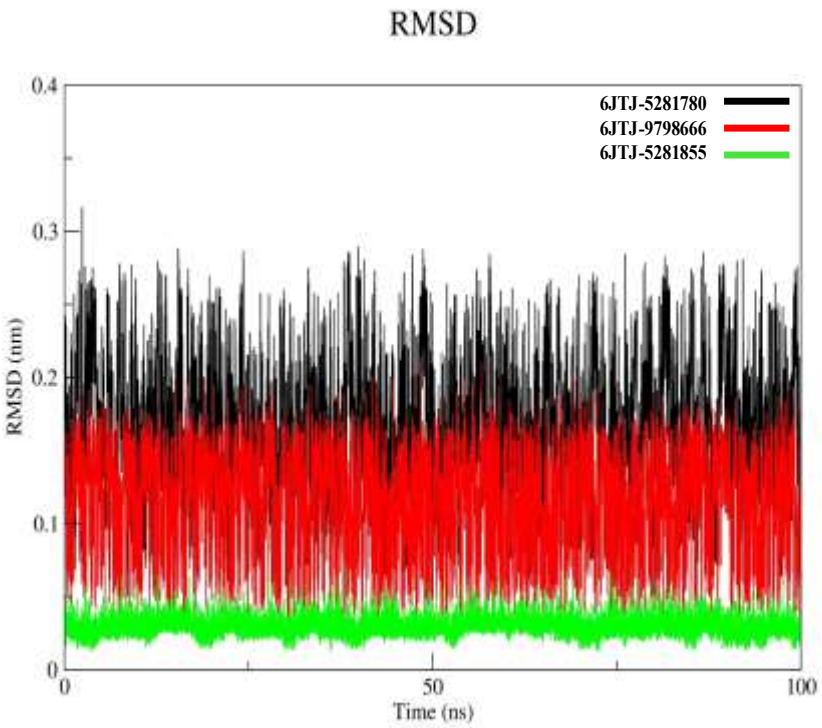

B. Root-mean-square fluctuation (RMSF)

Root-mean-square fluctuation (RMSF) analysis was performed to evaluate residue-level flexibility of the protein in complex with the three ligands (Figure 6.2). The 6JTJ–3,4-di-O-caffeoylquinic acid complex (CID: 5281780; black) exhibited the highest flexibility, with an average RMSF of 0.083 ± 0.051 nm and fluctuations ranging from 0.039 to 0.357 nm. Most residues remained below 0.11 nm; however, a pronounced peak was observed at residues 180–190, corresponding to the maximum fluctuation. Additional moderate fluctuations were detected at residues 70–80 and 300–315, which are likely associated with loop or surface-exposed regions that commonly display increased atomic mobility (Bagewadi et al., 2023; Song et al., 2024). Despite these localized fluctuations, the overall RMSF profile suggests that the protein maintained structural stability upon ligand binding, with

ISSN No. 2321-2705 | DOI: 10.51244/IJRSI |Volume XIII Issue VI June 2026

flexibility confined primarily to loop regions that may contribute to ligand accommodation or protein function (Martin & Frezza, 2022; Kuna et al., 2025).

The 6JTJ–cryptochlorogenic acid complex (CID: 9798666; red) demonstrated comparatively reduced flexibility, with an average RMSF of 0.073 ± 0.034 nm and a fluctuation range of 0.038–0.261 nm. Majority of residues were confined below 0.11 nm, indicating restricted backbone motion and moderate structural stabilization. The highest fluctuation was observed in the 300–310 region, with additional moderate peaks at residues 180–190 and 330–335. This is further supported by the study of Alsaady et al. (2026), who noted that ligand-bound proteins generally maintain conformational stability while flexibility remains localized in surface-exposed loops and terminal regions.

Among the complexes, the 6JTJ–ellagic acid complex (CID: 5281855; green) exhibited the lowest flexibility, with an average RMSF of 0.069 ± 0.025 nm and fluctuations ranging from 0.039 to 0.205 nm. Most residues were maintained below 0.095 nm, reflecting constrained atomic motion and enhanced structural rigidity upon ligand binding (Alsaady et al., 2026). Elevated fluctuations were primarily limited to residues 300–310, the C-terminal region, and moderate peaks around residues 180–185, while the remaining backbone regions remained comparatively rigid.

Overall, the RMSF profiles demonstrated a consistent reduction in residue-level fluctuations from the black to red to green systems, indicating increasing protein stabilization in the order of 3,4-di-O-caffeoylquinic acid, cryptochlorogenic acid, and ellagic acid. The lower RMSF values observed in the ellagic acid complex suggest enhanced structural stability and ligand-induced rigidity, consistent with previous studies associating reduced RMSF values with stable protein–ligand interactions (Song et al., 2024; Alsaady et al., 2026).

Figure 5. Residue-wise RMSF profile of the 6JTJ complexes.

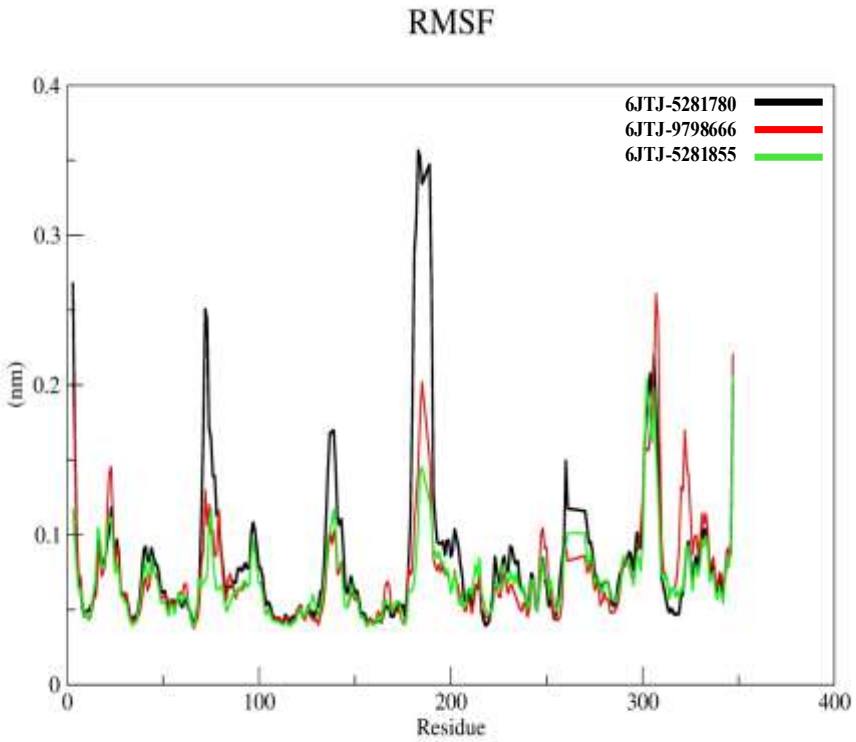

C. Radius of gyration

The radius of gyration (Rg) was analyzed to evaluate the overall compactness of the protein–ligand complexes. All three systems exhibited closely overlapping Rg profiles with minimal variation, indicating preservation of the global fold throughout the simulation (Ghahremanian et al., 2022; Maruyama & Mitsutake, 2022). The 6JTJ–

ISSN No. 2321-2705 | DOI: 10.51244/IJRSI |Volume XIII Issue VI June 2026

3,4-di-O-caffeoylquinic acid complex showed an average Rg of 1.975 ± 0.008 nm, the 6JTJ–cryptochlorogenic acid complex exhibited 1.977 ± 0.006 nm, and the 6JTJ–ellagic acid complex displayed 1.974 ± 0.008 nm. All systems remained confined within a narrow Rg window (~1.95–2.00 nm), with only minor fluctuations and no consistent expansion or contraction trend, indicating maintenance of structural compactness and stable protein conformation throughout the simulation (Ghahremanian et al., 2022; Maruyama & Mitsutake, 2022). Although the ellagic acid complex showed a marginal increase toward the later stage, the variation remained within the overall stable range. Tripathi et al. (2025) further noted that fluctuations within a narrow range indicate overall compactness and structural stability, while slight increases in Rg can reflect minor conformational changes or flexibility in the complex. Overall, ligand binding did not induce significant global conformational changes, and all complexes retained structural integrity and conformational stability throughout the simulation (Bagewadi et al., 2023).

Figure 6. Radius of gyration (Rg) of the 6JTJ complexes during the 100 ns MD simulation.

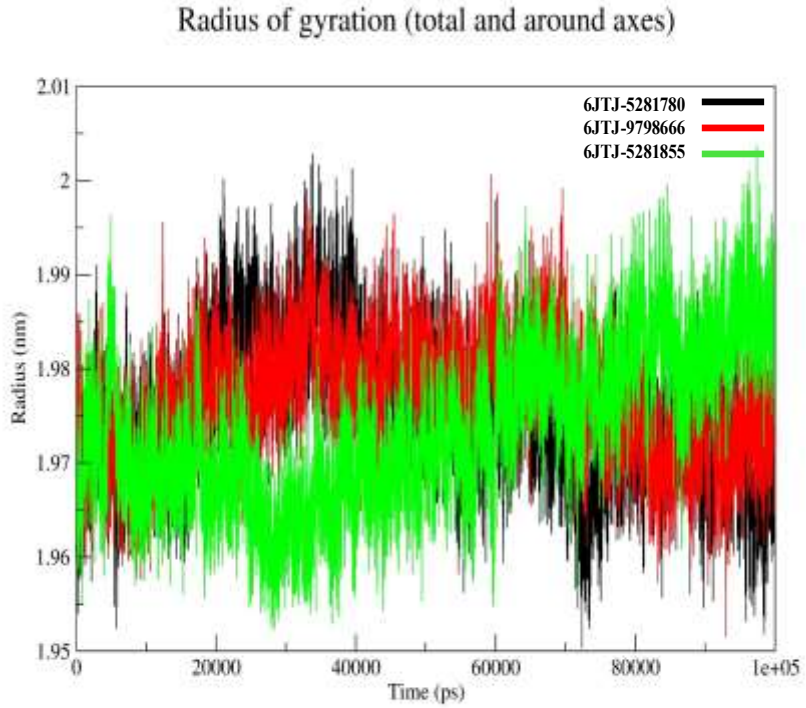

D. Solvent Accessible Surface Area

Solvent-accessible surface area (SASA) was analyzed to evaluate changes in the solvent-exposed regions of the protein–ligand complexes. All systems exhibited comparable SASA profiles with moderate fluctuations confined within a narrow range, indicating the absence of major conformational expansion or collapse. The 6JTJ–3,4-di-O-caffeoylquinic acid complex showed an average SASA of 149.420 ± 2.631 nm², the 6JTJ–cryptochlorogenic acid complex exhibited 148.056 ± 2.230 nm², and the 6JTJ–ellagic acid complex displayed 148.411 ± 2.301 nm². Temporary fluctuations were observed between 20–40 ns in the black system, 60–70 ns in the red system, and during the later stage in the green system; however, the overall SASA remained within a confined range (~140–158 nm²), indicating preservation of the overall solvent-accessible profile and absence of significant structural rearrangement. K and Venugopal (2024) reported that temporary SASA elevations typically reflect short-term outward residue movements without indicating structural instability, while Alsaady et al. (2026) noted that narrower SASA fluctuations often reflect more compact and stable protein–ligand interfaces. The slightly lower mean SASA and reduced fluctuation amplitude observed in the red and green systems suggest more consistent solvent exposure relative to the black system. Overall, the stable SASA distributions support maintenance of conformational stability throughout the MD simulations (K and Venugopal, 2024; Alsaady et al., 2026).

ISSN No. 2321-2705 | DOI: 10.51244/IJRSI |Volume XIII Issue VI June 2026

Figure 7. Solvent-accessible surface area (SASA) of the 6JTJ-ligand complexes.

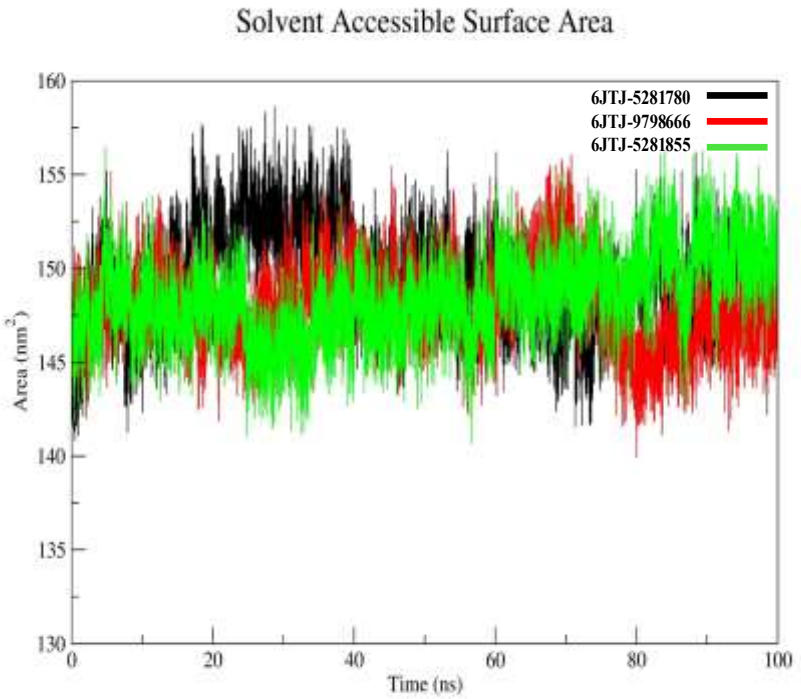

M. Hydrogen Bond Analysis

Hydrogen bond analysis was performed to evaluate ligand–protein interactions contributing to complex stability over the simulation period (Figure 6.5). Distinct interaction patterns were observed among the three systems, reflecting differences in the persistence and frequency of hydrogen bonding. The 6JTJ–3,4-di-O-caffeoylquinic acid complex (CID: 5281780; black) exhibited the highest hydrogen bond occupancy, with an average of ~2 interactions and a range of 0–5.

Most of the trajectory maintained 1–3 hydrogen bonds, with intermittent increases to 4–5, indicating recurring stabilization through polar interactions. The relatively consistent presence of multiple hydrogen bonds suggests sustained ligand–protein contact throughout the simulation, which is consistent with literature showing that ligands with stable multi-dentate hydrogen bonding often exhibit enhanced binding persistence and MM/MD stability (Guo et al., 2024).

The 6JTJ–cryptochlorogenic acid complex (CID: 9798666; red) showed a lower average of ~1 hydrogen bond, with values ranging from 0 to 5, indicating that hydrogen bonding is less persistent and largely transient, contributing intermittently to complex stabilization (Edache et al., 2024). In contrast, the 6JTJ–ellagic acid complex (CID: 5281855; green) displayed minimal hydrogen bond formation, with an average close to 0 and values ranging from 0 to 4.

Despite this, the overall structural stability observed in other parameters suggests that the complex is stabilized primarily through non-polar interactions and stacking or hydrophobic contacts rather than sustained hydrogen bonding (Guo et al., 2024; Edache et al., 2024). Overall, the hydrogen bond profiles indicate a decreasing trend in interaction persistence from black to red to green systems. While the 3,4-di-O-caffeoylquinic acid complex relies more on consistent hydrogen bonding, the ellagic acid complex maintains stability with minimal contribution from hydrogen bonds, indicating differing interaction mechanisms underlying ligand binding.

Figure 8. Time evolution of hydrogen bonds during the 100 ns molecular dynamics simulation.

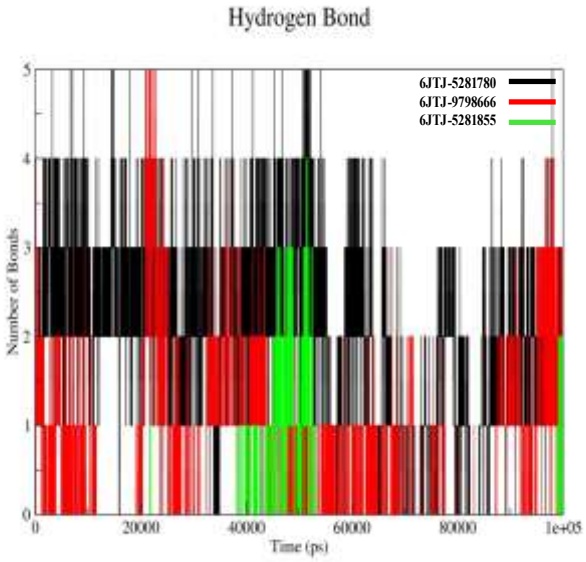

A. Molecular mechanics/Generalized born surface area

The binding free energies of the three protein–ligand complexes were estimated using the MM/GBSA approach, and the energetic components are summarized in Table 6.6 and Figure 6.6. All systems exhibited negative total binding energies, indicating favorable interactions, although with varying magnitudes and contributions from individual energy terms (Hassan et al., 2024). The 6JTJ–3,4-di-O-caffeoylquinic acid complex (CID: 5281780) showed a total binding free energy of −6.02 ± 7.79 kcal/mol. The gas-phase energy (GGAS: −59.37 ± 56.62 kcal/mol) was strongly favorable, dominated by electrostatic interactions (EEL: −52.04 ± 51.59 kcal/mol), while polar solvation (EGB: 54.70 ± 50.63 kcal/mol) substantially offset this favorable interaction, resulting in a moderately favorable total binding energy with high fluctuation. The 6JTJ–cryptochlorogenic acid complex (CID: 9798666) exhibited a slightly less favorable total binding free energy of −5.43 ± 6.79 kcal/mol, with contributions from both electrostatic (EEL: −7.83 ± 15.18 kcal/mol) and van der Waals interactions (VDWAALS: −9.47 ± 10.35 kcal/mol). The reduced gas-phase stabilization combined with moderate solvation penalty resulted in an overall weaker binding affinity.

In contrast, the 6JTJ–ellagic acid complex (CID: 5281855) showed the least favorable total binding free energy of −3.21 ± 5.84 kcal/mol. Despite a strong gas-phase interaction (GGAS: −49.27 ± 44.78 kcal/mol), primarily driven by electrostatic (EEL: −41.55 ± 38.35 kcal/mol) and van der Waals contributions (VDWAALS: −7.71 ± 8.7 kcal/mol), the binding was significantly counteracted by polar solvation (EGB: 47.31 ± 41.34 kcal/mol), reducing the overall binding affinity compared to the other complexes (Hassan et al., 2024). Comparatively, the total binding energies follow the trend: 3,4-di-O-caffeoylquinic acid > cryptochlorogenic acid > ellagic acid. In all cases, electrostatic interactions were the primary driving force for binding, while polar solvation opposed complex formation. The balance between these opposing contributions determined the overall binding affinity, with higher fluctuations in energy components reflecting dynamic interaction patterns throughout the simulation (Forouzesh & Mishra, 2021).

Table 8. MM/GBSA binding free energy components of the 6JTJ–complexes as mean ± SD (kcal/mol).

Components	Energies (kcal/mol)		
	6JTJ-5281780	**6JTJ-9798666**	**6JTJ-5281855**
VDWAALS	−7.32 ± 6.77	−9.47 ± 10.35	-7.71 ± 8.7
EEL	−52.04 ± 51.59	−7.83 ± 15.18	-41.55 ± 38.35
EGB	54.70 ± 50.63	13.07 ± 16.96	47.31 ± 41.34
ESURF	−1.35 ± 1.31	−1.19 ± 1.35	-1.26 ± 1.4

ISSN No. 2321-2705 | DOI: 10.51244/IJRSI |Volume XIII Issue VI June 2026

GGAS	−59.37 ± 56.62	−17.3 ± 21.92	-49.27 ± 44.78
GSOLV	53.34 ± 49.44	11.88 ± 15.87	46.05 ± 40.19
TOTAL	−6.02 ± 7.79	−5.43 ± 6.79	-3.21 ± 5.84

Figure 9. MM/GBSA binding free energy decomposition of the 6JTJ–ligand complexes

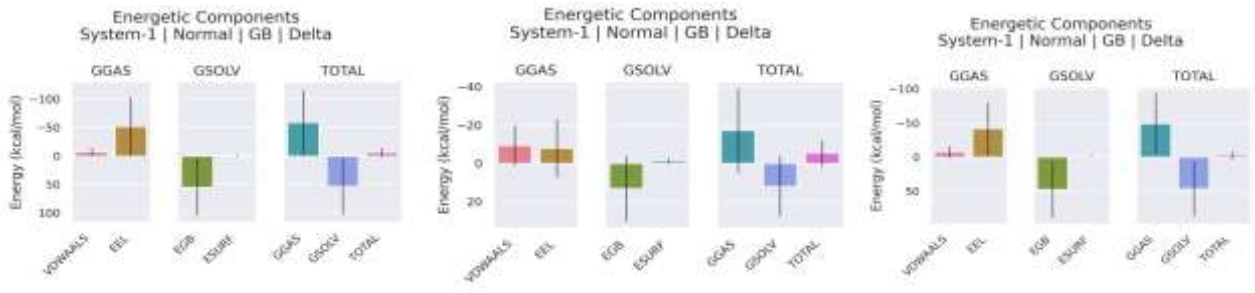

6JTJ-5281780 **6JTJ-9798666** **6JTJ-5281855**

CONCLUSION

This study comprehensively evaluated Philippine Fabaceae-derived phenolic acids as potential inhibitors of the NagZ enzyme of Neisseria gonorrhoeae through integrated in silico approaches, including molecular docking, drug-likeness assessment, ADME profiling, toxicity prediction, interaction analysis, molecular dynamics (MD) simulation, and MM/GBSA binding energy calculations. Molecular docking revealed favorable binding affinities ranging from −5.70 to −9.70 kcal/mol, with ellagic acid, 3,4-di-O-caffeoylquinic acid, and 4-caffeoylquinic acid exhibiting the strongest interactions due to extensive hydrogen bonding, hydrophobic interactions, and van der Waals forces within the NagZ active site, while low standard deviation values across repeated docking trials confirmed the stability and reproducibility of ligand–protein interactions. Drug-likeness evaluation showed that most compounds satisfied Lipinski's Rule of Five, although some top-performing ligands deviated from Veber's rule because of elevated topological polar surface area (TPSA), potentially limiting oral bioavailability despite retaining promising structural and binding characteristics. ADME analysis demonstrated variable pharmacokinetic properties among the phenolic acids, where some compounds showed favorable intestinal absorption and permeability while highly polar or glycosylated compounds exhibited reduced passive diffusion; notably, ellagic acid displayed comparatively favorable absorption, and most ligands showed acceptable distribution profiles with minimal cytochrome P450 interactions and limited metabolic liabilities. Toxicity prediction further indicated generally low to moderate toxicity classifications, high LD_{50} values, and minimal mutagenic, cytotoxic, or immunotoxic risks, although some compounds demonstrated predicted hepatotoxicity or carcinogenicity requiring further experimental validation. MD simulation analyses confirmed the structural and thermodynamic stability of the top ligand–protein complexes through RMSD, RMSF, radius of gyration (Rg), solvent-accessible surface area (SASA), hydrogen bonding, and MM/GBSA evaluations, with the 6JTJ–ellagic acid complex exhibiting the greatest structural stability and lowest atomic fluctuations, 3,4-di-O-caffeoylquinic acid demonstrating greater conformational flexibility and persistent hydrogen bonding, and 4-caffeoylquinic acid showing intermediate stability; all complexes maintained compact conformations and thermodynamically favorable negative binding energies primarily driven by electrostatic interactions. Overall, the integration of computational analyses identified ellagic acid, 3,4-di-O-caffeoylquinic acid, and 4-caffeoylquinic acid as the most promising NagZ inhibitory candidates derived from diverse Fabaceae species,

including Cassia fistula, Medicago polymorpha, Caesalpinia pulcherrima, Clitoria ternatea, Cassia grandis, Parkia speciosa, Pongamia pinnata, Senegalia catechu, and Vigna umbellata, highlighting these medicinal plants as valuable pharmacological resources for the development of novel antibacterial agents against gonorrhea and warranting further in vitro and in vivo validation studies.

RECOMMENDATIONS

The findings of this study demonstrated that selected phenolic compounds exhibited favorable binding affinities, stable ligand–protein interactions, and acceptable pharmacokinetic profiles, highlighting their potential as candidate inhibitors of the NagZ enzyme of Neisseria gonorrhoeae. Among the evaluated ligands, ellagic acid, 3,4-di-O-caffeoylquinic acid, and 4-caffeoylquinic acid are strongly recommended for further investigation because of their superior binding characteristics and interaction stability. Their corresponding plant sources, including Cassia fistula, Cassia grandis, Caesalpinia pulcherrima, Clitoria ternatea, Parkia speciosa, Pongamia pinnata, Senegalia catechu, Vigna umbellata, and Medicago polymorpha, should also be prioritized as potential reservoirs of bioactive compounds for drug development. Further validation through in vitro and in vivo studies is necessary to confirm the biological activity, safety, toxicity, bioavailability, and therapeutic efficacy of these compounds under physiological conditions. Additional investigations, including cytotoxicity assays, enzyme inhibition studies, and animal models, are recommended to evaluate dosage and possible adverse effects. Structural optimization may also be explored to improve pharmacokinetic properties while preserving binding affinity and interaction stability. Moreover, expanding future studies to include other antimicrobial resistance-related targets in Neisseria gonorrhoeae may contribute to the development of multi-target therapeutic strategies. Overall, this study provides a strong computational foundation for the continued development and experimental validation of these ligands as potential NagZ inhibitors.

REFERENCES

1. Abraham, M. J., Murtola, T., Schulz, R., Páll, S., Smith, J. C., Hess, B., & Lindahl, E. (2015). GROMACS: High performance molecular simulations through multi-level parallelism from laptops to supercomputers. SoftwareX, 1, 19–25.
2. Alsaady, I. M., Gattan, H. S., Aljahdali, S. M., Alruhaili, M. H., Dwivedi, V. D., & Azhar, E. I. (2026). Conformational dynamics and binding free energy analyses unveil a stable flavonoid inhibitor of dengue virus NS5 polymerase. Scientific Reports, 16(1). https://doi.org/10.1038/s41598-026-38864-2
3. AlSheikh, H. M. A., Sultan, I., Kumar, V., Rather, I. A., Al-Sheikh, H., Jan, A. T., & Haq, Q. M. R. (2020). Plant-Based phytochemicals as possible alternative to antibiotics in combating bacterial drug resistance. Antibiotics, 9(8), 480. https://doi.org/10.3390/antibiotics9080480
4. Asma, S. T., Imre, K., Morar, A., Herman, V., Acaroz, U., Mukhtar, H., Arslan-Acaroz, D., Shah, S. R., & Gerlach, R. (2022). An overview of biofilm formation–combating strategies and mechanisms of action of antibiofilm agents. Life, 12(8), 1110. https://doi.org/10.3390/life12081110
5. Azzam, K.A., 2023. SwissADME and pkCSM Webservers Predictors: an integrated Online Platform for Accurate and Comprehensive Predictions for In Silico ADME/T Properties of Artemisinin and its Derivatives. Kompleksnoe Ispolzovanie Mineralnogo Syra = Complex use of mineral resources 325, 14–21. https://doi.org/10.31643/2023/6445.13
6. Bagewadi, Z. K., Khan, T. Y., Gangadharappa, B., Kamalapurkar, A., Shamsudeen, S. M., & Yaraguppi, D. A. (2023). Molecular dynamics and simulation analysis against superoxide dismutase (SOD) target of Micrococcus luteus with secondary metabolites from Bacillus licheniformis recognized by genome mining approach. Saudi Journal of Biological Sciences, 30(9), 103753. https://doi.org/10.1016/j.sjbs.2023.103753
7. Baldwin, R. L., & Rose, G. D. (2016). How the hydrophobic factor drives protein folding. Proceedings of the National Academy of Sciences, 113(44), 12462–12466. https://doi.org/10.1073/pnas.1610541113
8. Bano, S., & Malik, J. K. (2022). Chlorogenic acid as a potential anti-inflammatory agent: An in-silico molecular docking approach. Middle East Research Journal of Pharmaceutical Sciences, 2(1), 10–20. https://doi.org/10.36348/merjps.2022.v02i01.002

9. Baruah, I., Kashyap, C., Guha, A. K., & Borgohain, G. (2022). Insights into the interaction between polyphenols and β-lactoglobulin through molecular docking, molecular dynamics simulation, and QM/MM approaches. ACS Omega, 7(27), 23083–23095. https://doi.org/10.1021/acsomega.2c00336
10. Bhoopalan, S. V., Piekarowicz, A., Lenz, J. D., Dillard, J. P., & Stein, D. C. (2016). Nagz triggers gonococcal biofilm disassembly. Scientific Reports, 6(1). https://doi.org/10.1038/srep22372
11. Brunner, K. (2024, June 29). Three benefits of using in silico technologies for drug discovery. Pharma's Almanac. https://www.pharmasalmanac.com/articles/three-benefits-of-using-in-silico-technologies-for-drug-discovery
12. C, S., S, D. K., Ragunathan, V., Tiwari, P., A, S., & P, B. D. (2022). Molecular docking, validation, dynamics simulations, and pharmacokinetic prediction of natural compounds against the SARS-CoV-2 main-protease. Journal of biomolecular structure & dynamics, 40(2), 585–611. https://doi.org/10.1080/07391102.2020.1815584
13. Chen P, Zou F and Liu W (2025) Recent advancement in prevention against hepatotoxicity, molecular mechanisms, and bioavailability of gallic acid, a natural phenolic compound: challenges and perspectives. Front. Pharmacol. 16:1549526. doi: 10.3389/fphar.2025.1549526
14. Chen, Y. (2019). Crystal structure of NagZ from Neisseria gonorrhoeae in complex with N-acetylglucosamine (PDB ID: 6JTJ) [Data set]. Worldwide Protein Data Bank. https://doi.org/10.2210/pdb6jtj/pdb
15. Clifford, M. N., Kerimi, A., & Williamson, G. (2020). Bioavailability and metabolism of chlorogenic acids (acyl-quinic acids) in humans. Comprehensive Reviews in Food Science and Food Safety, 19(4), 1299–1352. https://doi.org/10.1111/1541-4337.12518
16. Cornelissen, F. M. G., Markert, G., Deutsch, G., Antonara, M., Faaij, N., Bartelink, I., Noske, D., Vandertop, W. P., Bender, A., & Westerman, B. A. (2023). Explaining Blood-Brain Barrier Permeability of Small Molecules by Integrated Analysis of Different Transport Mechanisms. Journal of medicinal chemistry, 66(11), 7253–7267. https://doi.org/10.1021/acs.jmedchem.2c01824
17. Cosme, P., Rodríguez, A. B., Espino, J., & Garrido, M. (2020). Plant Phenolics: Bioavailability as a key determinant of their potential Health-Promoting applications. Antioxidants, 9(12), 1263. https://doi.org/10.3390/antiox9121263
18. Daina, A., Michielin, O., & Zoete, V. (2017). SwissADME: a free web tool to evaluate pharmacokinetics, drug-likeness and medicinal chemistry friendliness of small molecules. Scientific Reports, 7(1), 42717. https://doi.org/10.1038/srep42717
19. Dallakyan, S., Olson, A.J., 2015. Small-Molecule Library Screening by Docking with PyRx, in: Hempel, J.E., Williams, C.H., Hong, C.C. (Eds.), Chemical Biology, Methods in Molecular Biology. Springer New York, New York, NY, pp. 243–250. https://doi.org/10.1007/978-1-4939- 2269-7_19
20. De Barros Rêgo, C. M. V., Rahman, Z. M., Aguiar, A. P., Santos, T. F. F. D., Senar, S., Campos, L. A., & Baltatu, O. C. (2026). Cross-Database characterization of flavonoids and phenolic acids: integrating drug-likeness metrics, molecular interactions, and dietary sources. Molecules, 31(4), 728. https://doi.org/10.3390/molecules31040728
21. Department of Health. (2025). gonorrhea cases in the SOCCKSARGEN region [Unpublished raw data]. Republic of the Philippines.
22. Edache, E. I., Adedayo, A., Dawi, H. A., & Ugbe, F. A. (2024). Drug-like screening, molecular docking, molecular dynamics simulations, and binding free energies on the interaction of pyrazole derivatives as inhibitors of lysosomal storage disorders and anticancer activity. Discover Chemistry, 1, Article 22. https://doi.org/10.1007/s44371-024-00025-7
23. Ercan, S., & Şenses, Y. (2020). Design and molecular docking studies of new inhibitor candidates for EBNA1 DNA binding site: A computational study. Molecular Simulation, 46(4), 332–339. https://doi.org/10.1080/08927022.2019.1709638
24. Fekadu, M., Zeleke, D., Abdi, B., Guttula, A., Eswaramoorthy, R., & Melaku, Y. (2022). Synthesis, in silico molecular docking analysis, pharmacokinetic properties and evaluation of antibacterial and antioxidant activities of fluoroquinolines. BMC Chemistry, 16(1), 1. https://doi.org/10.1186/s13065-022-00795-0
25. Ferenczy, G. G., & Kellermayer, M. (2022). Contribution of hydrophobic interactions to protein mechanical stability. Computational and Structural Biotechnology Journal, 20, 1946–1956. https://doi.org/10.1016/j.csbj.2022.04.025

26. Forouzesh, N., & Mishra, N. (2021). An effective MM/GBSA protocol for absolute binding free energy calculations: A case study on SARS-COV-2 spike protein and the human ACE2 receptor. Molecules, 26(8), 2383. https://doi.org/10.3390/molecules26082383
27. Ghahremanian, S., Rashidi, M. M., Raeisi, K., & Toghraie, D. (2022). Molecular dynamics simulation approach for discovering potential inhibitors against SARS-CoV-2: A structural review. Journal of Molecular Liquids, 354, 118901. https://doi.org/10.1016/j.molliq.2022.118901
28. Golparian, D., & Unemo, M. (2022). Antimicrobial resistance prediction in neisseria gonorrhoeae: Current status and future prospects. Expert Review of Molecular Diagnostics, 22(1), 29–48. https://doi.org/10.1080/14737159.2022.2015329
29. Grgić, J., Šelo, G., Planinić, M., Tišma, M., & Bucić-Kojić, A. (2020). Role of the encapsulation in bioavailability of phenolic compounds. Antioxidants, 9(10), 923. https://doi.org/10.3390/antiox9100923
30. Guo, Y., Tong, J., Liang, J., Shi, K., Song, X., Guo, Z., Liu, B., & Xu, J. (2024b). Molecular insight into binding affinities and blockade effects of selected flavonoid compounds on the PD-1/PD-L1 pathway. RSC Advances, 14(36), 25908–25917. https://doi.org/10.1039/d4ra03877k
31. Guterres, H., & Im, W. (2020). Improving Protein-Ligand Docking Results with High-Throughput Molecular Dynamics Simulations. Journal of Chemical Information and Modeling, 60(4), 2189–2198. https://doi.org/10.1021/acs.jcim.0c00057
32. Gutiérrez-Durán, P. R., Horta-Vega, J. V., Olazarán-Santibáñez, F. E., Flores-Gracia, J., & Barrios-García, H. B. (2026). Phytochemical diversity and antimicrobial potential of Fabaceae species occurring in Tamaulipas, Mexico: a systematic review. Plants, 15(2), 278. https://doi.org/10.3390/plants15020278
33. Hassan, A. M., Gattan, H. S., Faizo, A. A., Alruhaili, M. H., Alharbi, A. S., Bajrai, L. H., Al-Zahrani, I. A., Dwivedi, V. D., & Azhar, E. I. (2024c). Evaluating the Binding Potential and Stability of Drug-like Compounds with the Monkeypox Virus VP39 Protein Using Molecular Dynamics Simulations and Free Energy Analysis. Pharmaceuticals, 17(12), 1617. https://doi.org/10.3390/ph17121617
34. K, D., & Venugopal, S. (2024). Molecular docking and molecular dynamic simulation studies to identify potential terpenes against Internalin A protein of Listeria monocytogenes. Frontiers in Bioinformatics, 4, 1463750. https://doi.org/10.3389/fbinf.2024.1463750
35. K, D., & Venugopal, S. (2024b). Molecular docking and molecular dynamic simulation studies to identify potential terpenes against Internalin A protein of Listeria monocytogenes. Frontiers in Bioinformatics, 4, 1463750. https://doi.org/10.3389/fbinf.2024.1463750
36. Ke, Q., Gong, X., Liao, S., Duan, C., & Li, L. (2022). Effects of thermostats/barostats on physical properties of liquids by molecular dynamics simulations. Journal of Molecular Liquids, 365, 120116. https://doi.org/10.1016/j.molliq.2022.120116
37. Kiokias, S., & Oreopoulou, V. (2021). A Review of the Health Protective Effects of Phenolic Acids against a Range of Severe Pathologic Conditions (Including Coronavirus-Based Infections). Molecules, 26(17), 5405. https://doi.org/10.3390/molecules26175405
38. Kiriyama, Y., Tokumaru, H., Sadamoto, H., Kobayashi, S., & Nochi, H. (2024). Effects of Phenolic Acids Produced from Food-Derived Flavonoids and Amino Acids by the Gut Microbiota on Health and Disease. Molecules, 29(21), 5102. https://doi.org/10.3390/molecules29215102
39. Kuna, K., Ganta, S., Akkiraju, P. C., Dokuparthi, S. K., India, B. P. P. L. H. T. S., Hussain, S., & Enaganti, S. (2025). Molecular dynamics simulation analysis of a modelled spermidine synthase from Yersinia pseudotuberculosis docked with cyclohexylamine. Bioinformation, 21(2), 210–219. https://doi.org/10.6026/973206300210210
40. Lai, H., Wang, L., Qian, R., Huang, J., Zhou, P., Ye, G., Wu, F., Wu, F., Zeng, X., & Liu, W.,(2024). Interformer: an interaction-aware model for protein-ligand docking and affinity prediction. Nature Communications, 15(1), 10223. https://doi.org/10.1038/s41467-024-54440-6
41. Liu, J., Du, C., Beaman, H. T., & Monroe, M. B. B. (2020). Characterization of Phenolic Acid Antimicrobial and Antioxidant Structure–Property Relationships. Pharmaceutics, 12(5), 419. https://doi.org/10.3390/pharmaceutics12050419
42. Madushanka, A., Moura, R. T., Verma, N., & Kraka, E. (2023). Quantum Mechanical Assessment of Protein–Ligand Hydrogen Bond Strength Patterns: Insights from Semiempirical Tight-Binding and Local Vibrational Mode Theory. International Journal of Molecular Sciences, 24(7), 6311. https://doi.org/10.3390/ijms24076311

43. Magaña, A. A., Kamimura, N., Soumyanath, A., Stevens, J. F., & Maier, C. S. (2021). Caffeoylquinic acids: chemistry, biosynthesis, occurrence, analytical challenges, and bioactivity. The Plant Journal, 107(5), 1299–1319. https://doi.org/10.1111/tpj.15390
44. Mandal, M. K., & Domb, A. J. (2024). Antimicrobial Activities of Natural Bioactive Polyphenols. Pharmaceutics, 16(6), 718. https://doi.org/10.3390/pharmaceutics16060718
45. Martin, J., & Frezza, E. (2022). A dynamical view of protein-protein complexes: Studies by molecular dynamics simulations. Frontiers in Molecular Biosciences, 9, 970109. https://doi.org/10.3389/fmolb.2022.970109
46. Maruyama, Y., & Mitsutake, A. (2022). Structural stability Analysis of proteins using End-to-End Distance: a 3D-RISM approach. J — Multidisciplinary Scientific Journal, 5(1), 114–125. https://doi.org/10.3390/j5010009
47. Moaje, M. (2022). STI cases on the rise in Quezon City. Philippine News Agency. https://www.pna.gov.ph/articles/1191393
48. Mohanty, M., & Mohanty, P. S. (2023). Molecular docking in organic, inorganic, and hybrid systems: a tutorial review. Monatshefte Für Chemie - Chemical Monthly, 154(7), 683–707. https://doi.org/10.1007/s00706-023-03076-1
49. Mongalo, N. I., & Raletsena, M. V. (2023). Fabaceae: South African Medicinal Plant Species Used in the Treatment and Management of Sexually Transmitted and Related Opportunistic Infections Associated with HIV-AIDS. Data, 8(11), 160. https://doi.org/10.3390/data8110160
50. Murugaiyan, J., Kumar, P. A., Rao, G. S., Iskandar, K., Hawser, S., Hays, J. P., Mohsen, Y., Adukkadukkam, S., Awuah, W. A., Jose, R. A. M., Sylvia, N., Nansubuga, E. P., Tilocca, B., Roncada, P., Roson-Calero, N., Moreno-Morales, J., Amin, R., Kumar, B. K., Kumar, A., Toufik, A. R., & Van Dongen, M. B. M. (2022). Progress in Alternative Strategies to Combat Antimicrobial Resistance: Focus on Antibiotics. Antibiotics (Basel, Switzerland), 11(2), 200. https://doi.org/10.3390/antibiotics11020200
51. Nivatya, H. K., Singh, A., Kumar, N., Sonam, Sharma, L., Singh, V., Mishra, R., Gaur, N., & Mishra, A. K. (2025). Assessing molecular docking tools: understanding drug discovery and design. Future Journal of Pharmaceutical Sciences, 11(1). https://doi.org/10.1186/s43094-025-00862-y
52. Obistioiu, D., Cocan, I., Tîrziu, E., Herman, V., Negrea, M., Cucerzan, A., Neacsu, A.-G., Cozma, A. L., Nichita, I., Hulea, A., Radulov, I., & Alexa, E. (2021). Phytochemical profile and microbiological activity of some plants belonging to the Fabaceae family. Antibiotics, 10(6), 662. https://doi.org/10.3390/antibiotics10060662
53. Páll, S., Zhmurov, A., Bauer, P., Abraham, M., Lundborg, M., Gray, A., Hess, B., & Lindahl, E. (2020). Heterogeneous parallelization and acceleration of molecular dynamics simulations in GROMACS. The Journal of Chemical Physics, 153(13). https://pubs.aip.org/aip/jcp/article/153/13/134110/199476
54. Pinzi, L., & Rastelli, G. (2019). Molecular Docking: Shifting paradigms in drug discovery. International Journal of Molecular Sciences, 20(18), 4331. https://doi.org/10.3390/ijms20184331
55. Programmes, G. H. H. a. S. (2021, July 15). Global progress report on HIV, viral hepatitis and sexually transmitted infections, 2021. https://www.who.int/publications/i/item/9789240027077
56. Programmes, G. H. H. a. S. (2021, July 15). Global progress report on HIV, viral hepatitis and sexually transmitted infections, 2021. https://www.who.int/publications/i/item/9789240027077
57. Purohit, R. (2014). Role of ELA region in auto-activation of mutant KIT receptor: A molecular dynamics simulation insight. Journal of Biomolecular Structure and Dynamics, 32(7), 1033–1046. https://doi.org/10.1080/07391102.2013.803264
58. Rajendran, V., Gopalakrishnan, C., & Sethumadhavan, R. (2018). Pathological role of a point mutation (T315I) in BCR-ABL1 protein—A computational insight. Journal of Cellular Biochemistry, 119(1), 918–925. https://doi.org/10.1002/jcb.26257
59. Sadhukhan, S., Das, M., Mondal, P., Chakraborty, D., & Biswas, N. (2025). In Silico Molecular Docking, Validation, ADMET, and Drug Likeness Prediction of Phytochemicals Against Multiple Therapeutic Targets of Diabetes Mellitus: In Silico Evaluation of Antidiabetic Phytochemicals. Iranian Journal of Pharmaceutical Sciences, 21(1), 357–381. https://doi.org/10.22037/ijps.v21i1.47074
60. Sahu, M. K., Nayak, A. K., Hailemeskel, B., & Eyupoglu, O. E. (2024). Exploring Recent Updates on Molecular Docking: Types, Method, Application, Limitation & Future Prospects. International Journal of Pharmaceutical Research and Allied Sciences, 13(2), 24–40. https://doi.org/10.51847/une9jqjucl

61. Sarenje, K. L., Ngalamika, O., Maimbolwa, M. C., Siame, A., Munsaka, S. M., & Kwenda, G. (2022). Antimicrobial resistance of neisseria gonorrhoeae isolated from patients attending sexually transmitted infection clinics in urban hospitals, Lusaka, Zambia. BMC Infectious Diseases, 22(1). https://doi.org/10.1186/s12879-022-07674-y
62. Sasidharan, S., Gosu, V., Tripathi, T., & Saudagar, Prakash. (2023). Molecular Dynamics Simulation to Study Protein Conformation and Ligand Interaction. 10.1007/978-981-99-2079-2_6.
63. Sharif Ezzaz, A. (2024). A review on principles of molecular docking and its application in drug discovery (Doctoral dissertation, Brac University).
64. Sharma, J., Bhardwaj, V. K., Das, P., & Purohit, R. (2021). Identification of naturally originated molecules as γ-aminobutyric acid receptor antagonist. Journal of Biomolecular Structure and Dynamics, 39(3), 911–922. https://doi.org/10.1080/07391102.2020.1720818
65. Shivanika, C., Kumar, D., Ragunathan, V., Tiwari, P., & Sumitha, A. (2020) Molecular docking, validation, dynamics simulations, and pharmacokinetic prediction of natural compounds against the SARS-CoV-2 main-protease. Journal of Biomolecular Structure & Dynamics, 1.
66. Singh, R., Bhardwaj, V., & Purohit, R. (2021). Identification of a novel binding mechanism of Quinoline based molecules with lactate dehydrogenase of Plasmodium falciparum. Journal of Biomolecular Structure and Dynamics, 39(1), 348–356. https://doi.org/10.1080/07391102.2020.1711809
67. Song, X., Bao, L., Feng, C., Huang, Q., Zhang, F., Gao, X., & Han, R. (2024). Accurate prediction of protein structural flexibility by deep learning integrating intricate atomic structures and Cryo-EM density information. Nature Communications, 15(1), 5538. https://doi.org/10.1038/s41467-024-49858-x
68. Tariq, M., Ahmad, N., Nisa, M. U., Rahim, M. A., & Zongo, E. (2024). Phytochemicals profiling of Cassia fistula fruit extract and its effect on serum lipids and hematological parameters in high-fat diet-induced hyperlipidemic female rats. Food science & nutrition, 12(8), 5776–5784. https://doi.org/10.1002/fsn3.4229
69. Tripathi, K. L., Dwivedi, V. D., & Badoni, H. (2025). Pharmacophore modeling and molecular dynamics simulations to study the conformational stability of natural HER2 inhibitors in breast cancer therapy. Molecular Diversity, 30(1), 327–351. https://doi.org/10.1007/s11030-025-11165-y
70. Valdés-Tresanco, M. S., Valdés-Tresanco, M. E., Valiente, P. A., & Moreno, E. (2021). gmx_MMPBSA: A New Tool to Perform End-State Free Energy Calculations with GROMACS. Journal of Chemical Theory and Computation, 17(10), 6281–6291. https://doi.org/10.1021/acs.jctc.1c00645
71. Vidal de Barros Rêgo, C. M., Rahman, Z. M., Aguiar, A. P., Ferreira Dos Santos, T. F., Senar, S., Campos, L. A., & Baltatu, O. C. (2026). Cross-Database Characterization of Flavonoids and Phenolic Acids: Integrating Drug-likeness Metrics, Molecular Interactions, and Dietary Sources. Molecules (Basel, Switzerland), 31(4), 728. https://doi.org/10.3390/molecules31040728
72. Wojciechowski, M. (2017). Simplified AutoDock force field for hydrated binding sites. Journal of Molecular Graphics and Modelling, 78, 74–80. https://doi.org/10.1016/j.jmgm.2017.09.016
73. Yakobi, S., Zuma, L., Gasa, N., & Pooe, O. (2024). Antimicrobial Potential of Organic Phenolic Compounds from Wild Mushroom Extracts: Impact on Proliferation and Kinetic Growth of Multidrug-Resistant Neisseria gonorrhoeae Strains. Journal of Food Biochemistry, 2024(1). https://doi.org/10.1155/2024/2336255
74. Yang, X., Zeng, J., Wang, D., Zhou, Q., Yu, X., Wang, Z., Bai, T., Luan, G., & Xu, Y. (2024). NagZ modulates the virulence of E. cloacae by acting through the gene of unknown function, ECL_03795. Virulence, 15(1), 2367652. https://doi.org/10.1080/21505594.2024.2367652
75. Zhu, C., Lin, Z., Jiang, H., Wei, F., Wu, Y., & Song, L. (2024). Recent advances in the health benefits of phenolic acids in whole grains and the impact of processing techniques on phenolic acids: a Comprehensive review. Journal of Agricultural and Food Chemistry, 72(44), 24131–24157. https://doi.org/10.1021/acs.jafc.4c05245

ISSN No. 2321-2705 | DOI: 10.51244/IJRSI |Volume XIII Issue VI June 2026

Table 1. Binding Affinity

Binding Energy							Average
Ligands		Trial 1	Trial 2	Trial 3	Trial 4	Trial 5	
1	1-O-sinapoyl-beta-D-glucose	-8	-7.9	-8.1	-7.8	-7.9	-7.94
2	3-Hydroxybenzoic acid	-5.8	-5.8	-5.8	-5.8	-5.8	-5.80
3	3,4-di-O-caffeoylquinic acid	-8.7	-9.6	-9.1	-9.5	-9.6	-9.30
4	3,4-dihydroxy-trans-cinnamic acid	-6.6	-6.6	-6.6	-6.6	-6.6	-6.60
5	3,4-dihydroxybenzoic acid butyl ester	-7.2	-7.2	-7.2	-7.2	-7.2	-7.20
6	3,4-dihydroxybenzoic acid ethyl ester	-6	-5.9	-6	-6.2	-6.1	-6.04
7	3,4-dihydroxybenzoic acid methyl ester	-6	-5.9	-6	-6	-6	-5.98
8	4-Caffeoylquinic acid	-8.8	-8.8	-8.8	-8.8	-8.8	-8.80
9	4-Methoxycinnamic acid	-6.1	-6	-6	-5.8	-6	-5.98
10	5-Methoxysalicylic Acid	-6.1	-6.1	-6.1	-6.1	-6.1	-6.10
11	Caffeic acid	-6.2	-6.2	-6.3	-6.2	-6.2	-6.22
12	Chlorogenic acid	-8.2	-8.2	-8.2	-8.2	-8.2	-8.20
13	Cinnamic acid	-5.9	-5.9	-5.8	-5.9	-5.8	-5.86
14	D-3-Phenyllactic acid	-6	-6	-6.1	-6	-6	-6.02
15	Ellagic acid	-9.7	-9.7	-9.7	-9.7	-9.7	-9.70
16	Ethyl gallate	-6	-6.1	-6.1	-6.1	-6.1	-6.08
17	Ferulic acid	-6.2	-6.2	-6.2	-6.2	-6.2	-6.20
18	Gallic acid	-6.3	-6.3	-6.3	-6.3	-6.3	-6.30
19	Gallic acid ethyl ester	-6.1	-6.0	-6.0	-6.0	-6.0	-6.02
20	Gentisic acid	-6.0	-6.0	-6.0	-6.0	-6.0	-6.00
21	Hydroxybenzoic acid	-5.7	-5.7	-5.7	-5.7	-5.7	-5.70
22	Isovanillic acid	-6.3	-6.3	-6.3	-6.3	-6.3	-6.30
23	m-Coumaric acid	-6.2	-6.3	-6.3	-6.3	-6.3	-6.28
24	Methyl ferulate	-6.0	-6.1	-6.1	-6.1	-6.1	-6.08
25	Methyl gallate	-6.2	-6.2	-6.2	-6.2	-6.2	-6.20
26	o-Coumaric acid	-6.2	-6.2	-6.2	-6.2	-6.2	-6.20
27	p-Coumaric acid	-6.5	-6.5	-6.5	-6.5	-6.5	-6.50
28	p-Coumaric acid-O-glucoside	-7.8	-7.8	-7.8	-7.8	-7.8	-7.80
29	Protocatechuic acid	-6.1	-6.1	-6.1	-6.1	-6.1	-6.10
30	Protocatechuic acid methyl ester	-6	-6	-6	-6	-6	-6.00
31	Rosmarinic acid	-7.8	-7.6	-7.6	-8.5	-8	-7.90
32	Salicylic acid	-5.7	-5.7	-5.7	-5.7	-5.7	-5.70
33	Sinapic acid	-6.3	-6.4	-6.3	-6.4	-6.3	-6.34
34	Syringic acid	-5.7	-5.7	-5.7	-5.7	-5.9	-5.74
35	trans-Cinnamate	-5.8	-5.8	-5.8	-5.8	-5.8	-5.80
36	trans-Methyl p-coumarate	-6.1	-6.1	-6.1	-6.1	-6.1	-6.10
37	Vanillic acid	-6.1	-5.9	-5.9	-6.0	-5.9	-5.96

Table 2. Drug-likeness Properties

Compounds		MW (gm/mol)	NRB	NHA	NHD	TPSA ($Å^2$)	LogP (clogP)	Lipinski's rule violation	Veber's rule violation
1	1-O-sinapoyl-beta-D-glucose	386.35	7	10	5	155.14	-0.51	Accepted	Rejected
2	3-Hydroxybenzoic acid	138.12	1	3	2	57.53	1.03	Accepted	Accepted

ISSN No. 2321-2705 | DOI: 10.51244/IJRSI |Volume XIII Issue VI June 2026

3	**3,4-di-O-caffeoylquinic acid**	516.45	9	12	7	211.28	0.80	Rejected	Rejected
4	**3,4-dihydroxy-trans-cinnamic acid**	180.16	2	4	3	77.76	0.92	Accepted	Accepted
5	**3,4-dihydroxybenzoic acid butyl ester**	496.90	10	4	0	44.76	2.797	Accepted	Accepted
6	**3,4-dihydroxybenzoic acid ethyl ester**	182.17	3	4	2	66.76	1.40	Accepted	Accepted
7	**3,4-dihydroxybenzoic acid methyl ester**	168.15	2	4	2	66.76	1.07	Accepted	Accepted
8	**4-Caffeoylquinic acid**	354.31	5	9	6	164.75	-0.37	Accepted	Rejected
9	**4-Methoxycinnamic acid**	178.18	3	3	1	46.53	1.87	Accepted	Accepted
10	**5-Methoxysalicylic acid**	168.15	2	4	2	66.76	1.14	Accepted	Accepted
11	**Caffeic acid**	180.040	2	4	3	77.760	1.430	Accepted	Accepted
12	**Chlorogenic acid**	354.100	5	9	6	164.750	0.331	Accepted	Rejected
13	**Cinnamic acid**	148.050	2	2	1	37.300	1.970	Accepted	Accepted
14	**D-3-Phenyllactic acid**	166.060	3	3	2	57.530	0.701	Accepted	Accepted
15	**Ellagic acid**	302.010	0	8	4	141.340	1.117	Accepted	Rejected
16	**Ethyl gallate**	198.050	3	5	3	86.990	1.560	Accepted	Accepted
17	**Ferulic acid**	194.060	3	4	2	66.760	1.803	Accepted	Accepted
18	**Gallic acid**	170.020	1	5	4	97.990	0.645	Accepted	Accepted
19	**Gallic acid ethyl ester**	198.050	3	5	3	86.990	1.560	Accepted	Accepted
20	**Gentisic acid**	154.030	1	4	3	77.760	1.636	Accepted	Accepted
21	**Hydroxybenzoic acid**	138.030	1	3	2	57.530	1.510	Accepted	Accepted
22	**Isovanillic acid**	168.040	2	4	2	66.760	1.370	Accepted	Accepted
23	**m-Coumaric acid**	164.050	2	3	2	57.530	1.455	Accepted	Accepted
24	**Methyl ferulate**	208.070	4	4	1	55.760	2.269	Accepted	Accepted
25	**Methyl gallate**	184.040	2	5	3	86.990	1.033	Accepted	Accepted
26	**o-Coumaric acid**	164.050	2	3	2	57.530	2.182	Accepted	Accepted
27	**p-Coumaric acid**	164.050	2	3	2	57.530	1.923	Accepted	Accepted
28	**p-Coumaric acid-O-glucoside**	326.100	5	8	5	136.680	-0.308	Accepted	Accepted
29	**Protocatechuic acid**	154.030	1	4	3	77.760	1.041	Accepted	Accepted

30	**Protocatechuic acid methyl ester**	168.040	2	4	2	66.760	1.443	Accepted	Accepted
31	**Rosmarinic acid**	360.080	7	8	5	144.520	1.775	Accepted	Accepted
32	**Salicylic acid**	138.030	1	3	2	57.530	2.221	Accepted	Accepted
33	**Sinapic acid**	224.070	4	5	2	75.990	1.572	Accepted	Accepted
34	**Syringic acid**	198.050	3	5	2	75.990	1.212	Accepted	Accepted
35	**trans-Cinnamate**	148.050	2	2	1	37.300	1.970	Accepted	Accepted
36	**trans-Methyl p-coumarate**	178.060	3	3	1	46.530	2.325	Accepted	Accepted
37	**Vanillic acid**	168.15	2	4	2	66.76	1.08	Accepted	Accepted

Table 3. Pharmacokinetic properties (ADME)

COMPOUNDS		**ABSORPOTION**				**DISTRIBUTION**				**METABOLISM**	**EXCRETION**	
		Water solubility (log mol/L)	**Caco2 Permeability (log Papp in 10-6 cm/s)**	**HIA (% Absorbed)**	**Skin Permeability (log Kp)**	**VDss (human) (log L/kg)**	**Fraction unbound (human) (Fu)**	**BBB permeability (log BB)**	**CNS permeability (log PS)**	**CYP2D6 substrate CYP3A4 substrate CYP1A2 inhibitor CYP2C19 inhibitor CYP2C9 inhibitor**	**Total Clearance (log ml/min/kg)**	**Renal OCT2 substrate**
1	**1-O-sinapoyl-beta-D-glucose**	-1.961	0.172	47.505	-2.744	-0.005	-0.005	-1.308	-4.05	No; No; No; No; No	0.71	No
2	**3-Hydroxybenzoic acid**	-1.98	1.123	79.081	-2.735	-1.607	0.605	-0.397	-2.86	No; No; No; No; No	0.588	No
3	**3,4-di-O-caffeoylquinic acid**	-2.955	-1.203	29.037	-2.735	-2.735	0.294	-2.08	-3.804	No; Yes; No; No; No	-0.042	No
4	**3,4-dihydroxy-trans-cinnamic acid**	-2.33	0.634	69.407	-2.722	-1.098	0.529	-0.647	-2.608	No; No; No; No; No	0.508	No
5	**3,4-dihydroxybenzoic acid butyl ester**	-8.629	1.316	88.84	-2.652	0.245	0	-0.377	-1.65	No; Yes; No; No; Yes	0.243	No
6	**3,4-dihydroxybenzoic acid ethyl ester**	-2.094	0.05	83.434	-2.996	0.228	0.538	-0.362	-2.941	No; No; Yes; No; No	0.708	No
7	**3,4-dihydroxybenzoic acid methyl ester**	-1.981	-0.001	83.368	-2.998	0.163	0.552	-0.39	-2.942	No; No; No; No; No	0.669	No
8	**4-Caffeoylquinic acid**	-2.428	-0.892	20.029	-2.735	0.546	0.662	-1.593	-3.791	No; No; No; No; No	0.298	No
9	**4-Methoxycinnamic acid**	-2.945	1.236	94.977	-2.708	-1.182	0.305	0.312	-2.085	No; No; No; No; No	0.766	No
10	**5-Methoxysalicylic acid**	-2.139	0.359	77.879	-2.735	-1.617	0.563	-0.409	-2.559	No; No; No; No; No	0.651	No
11	**Caffeic acid**	-2.33	0.634	69.407	-2.722	-1.098	0.529	-0.647	-2.608	No; No; No; No; No	0.508	No
12	**Chlorogenic acid**	-2.449	-0.84	36.377	-2.735	0.581	0.658	-1.407	-3.856	No; No; No; No; No	0.307	No
13	**Cinnamic acid**	-2.608	1.717	94.833	-2.695	-1.501	0.38	0.446	-1.834	No; No; No; No; No	0.781	No
14	**D-3-Phenyllactic acid**	-2.139	1.162	78.543	-2.715	-0.994	0.549	-0.229	-2.686	No; No; No; No; No	0.72	No
15	**Ellagic acid**	-3.181	0.335	86.684	-2.735	0.375	0.083	-1.272	-3.533	No; No; Yes; No; No	0.537	No

16	**Ethyl gallate**	-2.043	-0.004	76.701	-2.771	0.405	0.605	-1.098	-3.376	No; No; No; No; No	0.674	No
17	**Ferulic acid**	-2.817	0.176	93.685	-2.72	-1.367	0.343	-0.239	-2.612	No; No; No; No; No	0.623	No
18	**Gallic acid**	-2.56	-0.081	43.374	-2.735	-1.855	0.617	-1.102	-3.74	No; No; No; No; No	0.518	No
19	**Gallic acid ethyl ester**	-2.043	-0.004	76.701	-2.771	0.405	0.605	-1.098	-3.376	No; No; No; No; No	0.674	No
20	**Gentisic acid**	-2.009	0.542	80.078	-2.735	-1.515	0.689	-0.697	-3.283	No; No; No; No; No	0.587	No
21	**Hydroxybenzoic acid**	-1.877	1.151	83.961	-2.723	-1.557	0.592	-0.334	-3.21	No; No; No; No; No	0.593	No
22	**Isovanillic acid**	-1.826	0.295	88.094	-2.73	-1.843	0.516	-0.38	-2.628	No; No; No; No; No	0.626	No
23	**m-Coumaric acid**	-2.538	1.196	92.864	-2.709	-1.16	0.501	-0.287	-2.351	No; No; No; No; No	0.663	No
24	**Methyl ferulate**	-1.916	1.253	92.407	-2.724	-0.166	0.272	0.413	-2.463	No; No; Yes; No; No	0.649	No
25	**Methyl gallate**	-2	-0.056	76.635	-2.771	0.355	0.615	-1.046	-3.376	No; No; No; No; No	0.635	No
26	**o-Coumaric acid**	-2.419	1.21	93.494	-2.712	-1.191	0.424	-0.225	-2.418	No; No; No; No; No	0.736	No
27	**p-Coumaric acid**	-2.378	1.21	93.494	-2.715	-1.151	0.428	-0.225	–2.418	No; No; No; No; No	0.662	No
28	**p-Coumaric acid-O-glucoside**	-2.393	-0.585	14.12	-2.735	-0.718	0.627	-1.076	-3.851	No; No; No; No; No	0.278	No
29	**Protocatechuic acid**	-2.069	0.49	71.174	-2.727	-1.298	0.648	-0.683	-3.305	No; No; No; No; No	0.551	No
30	**Protocatechuic acid methyl ester**	-1.981	-0.001	83.368	-2.998	0.163	0.552	-0.39	-2.942	No; No; No; No; No	0.669	No
31	**Rosmarinic acid**	-3.059	-0.937	32.516	-2.735	0.393	0.348	-1.378	-3.347	No; No; No; No; No	0.25	No
32	**Salicylic acid**	-1.808	1.151	83.887	-2.723	-1.57	0.563	-0.334	-3.21	No; No; No; No; No	0.607	No
33	**Sinapic acid**	-2.869	0.272	93.064	-2.725	-1.11	0.45	-0.247	-2.663	No; No; No; No; No	0.718	No
34	**Syringic acid**	-2.223	0.495	73.076	-2.735	-1.443	0.601	-0.191	-2.701	No; No; No; No; No	0.646	No
35	**trans-Cinnamate**	-2.458	1.602	81.815	-2.705	-1.704	0.404	-0.082	-1.658	No; No; No; No; No	0.307	No
36	**trans-Methyl p-coumarate**	-1.662	1.203	94.708	-2.749	0.072	0.405	0.054	-2.053	No; No; Yes; No; No	0.686	No
37	**Vanillic acid**	-1.838	0.33	78.152	-2.726	-1.739	0.518	-0.38	-2.628	No; No; No; No; No	0.628	No

Table 4. Toxicity characteristics

Compounds		**LD50 (mg/kg)**	**Toxic Class**	**Organ Toxicity**				
				Hepatotoxicity	**Carcinogenicity**	**Immunotoxicity**	**Mutagenicity**	**Cytotoxicity**
1	**1-O-sinapoyl-beta-D-glucose**	5000mg/kg	5	Inactive	Inactive	Active	Inactive	Inactive
2	**3-Hydroxybenzoic acid**	2000mg/kg	4	Inactive	Inactive	Inactive	Inactive	Inactive
3	**3,4-di-O-caffeoylquinic acid**	5000mg/kg	5	Inactive	Inactive	Active	Inactive	Inactive
4	**3,4-dihydroxy-trans-cinnamic acid**	2980mg/kg	5	Inactive	Active	Inactive	Inactive	Inactive
5	**3,4-dihydroxybenzoic acid butyl ester**	2000mg/kg	4	Inactive	Inactive	Inactive	Inactive	Inactive
6	**3,4-dihydroxybenzoic acid ethyl ester**	5810mg/kg	6	Inactive	Inactive	Inactive	Inactive	Inactive
7	**3,4-dihydroxybenzoic acid methyl ester**	1700mg/kg	4	Inactive	Inactive	Inactive	Inactive	Inactive
8	**4-Caffeoylquinic acid**	5000mg/kg	5	Inactive	Inactive	Active	Inactive	Inactive

ISSN No. 2321-2705 | DOI: 10.51244/IJRSI |Volume XIII Issue VI June 2026

9	**4-Methoxycinnamic acid**	2980mg/kg	5	Active	Inactive	Inactive	Inactive	Inactive
10	**5-Methoxysalicylic acid**	2980mg/kg	5	Active	Inactive	Inactive	Inactive	Inactive
11	**Caffeic acid**	2980mg/kg	5	Inactive	Active	Inactive	Inactive	Inactive
12	**Chlorogenic acid**	5000mg/kg	5	Inactive	Inactive	Active	Inactive	Inactive
13	**Cinnamic acid**	2500mg/kg	5	Active	Inactive	Inactive	Inactive	Inactive
14	**D-3-Phenyllactic acid**	1154mg/kg	4	Inactive	Inactive	Inactive	Inactive	Inactive
15	**Ellagic acid**	2991mg/kg	4	Inactive	Active	Inactive	Inactive	Inactive
16	**Ethyl gallate**	5810mg/kg	6	Inactive	Inactive	Inactive	Inactive	Inactive
17	**Ferulic acid**	1772mg/kg	4	Inactive	Inactive	Active	Inactive	Inactive
18	**Gallic acid**	2000mg/kg	4	Inactive	Active	Inactive	Inactive	Inactive
19	**Gallic acid ethyl ester**	1190mg/kg	4	Active	Inactive	Active	Inactive	Inactive
20	**Gentisic acid**	4500mg/kg	5	Inactive	Inactive	Inactive	Inactive	Inactive
21	**Hydroxybenzoic acid**	2200mg/kg	5	Inactive	Inactive	Inactive	Inactive	Inactive
22	**Isovanillic acid**	2000mg/kg	4	Inactive	Inactive	Inactive	Inactive	Inactive
23	**m-Coumaric acid**	2980mg/kg	5	Inactive	Active	Inactive	Inactive	Inactive
24	**Methyl ferulate**	978mg/kg	4	Active	Inactive	Active	Inactive	Inactive
25	**Methyl gallate**	1700mg/kg	4	Inactive	Inactive	Inactive	Inactive	Inactive
26	**o-Coumaric acid**	2850mg/kg	5	Active	Active	Inactive	Inactive	Inactive
27	**p-Coumaric acid**	2850mg/kg	5	Inactive	Active	Inactive	Inactive	Inactive
28	**p-Coumaric acid-O-glucoside**	4000mg/kg	5	Inactive	Inactive	Active	Inactive	Inactive
29	**Protocatechuic acid**	2000mg/kg	4	Inactive	Active	Inactive	Inactive	Inactive
30	**Protocatechuic acid methyl ester**	1700mg/kg	4	Inactive	Inactive	Inactive	Inactive	Inactive
31	**Rosmarinic acid**	5000mg/kg	5	Inactive	Inactive	Active	Inactive	Inactive
32	**Salicylic acid**	1034mg/kg	4	Active	Inactive	Inactive	Inactive	Inactive
33	**Sinapic acid**	1772mg/kg	4	Inactive	Inactive	Active	Inactive	Inactive
34	**Syringic acid**	1700mg/kg	4	Inactive	Inactive	Inactive	Inactive	Inactive
35	**trans-Cinnamate**	2500mg/kg	5	Inactive	Inactive	Inactive	Inactive	Inactive
36	**trans-Methyl p-coumarate**	2850mg/kg	5	Active	Inactive	Inactive	Inactive	Inactive
37	**Vanillic acid**	2000mg/kg	4	Inactive	Inactive	Inactive	Inactive	Inactive

Table 5. Descriptive statistics of the binding affinity values

Binding Energy							**Average**	**Standard Deviation**
Ligands		**Trial 1**	**Trial 2**	**Trial 3**	**Trial 4**	**Trial 5**		
1	**1-O-sinapoyl-beta-D-glucose**	**-8**	**-7.9**	**-8.1**	**-7.8**	**-7.9**	**-7.94**	**0.1140**
2	**3-Hydroxybenzoic acid**	**-5.8**	**-5.8**	**-5.8**	**-5.8**	**-5.8**	**-5.80**	**0.0000**
3	**3,4-di-O-caffeoylquinic acid**	**-8.7**	**-9.6**	**-9.1**	**-9.5**	**-9.6**	**-9.30**	**0.3937**
4	**3,4-dihydroxy-trans-cinnamic acid**	**-6.6**	**-6.6**	**-6.6**	**-6.6**	**-6.6**	**-6.60**	**0.0000**
5	**3,4-dihydroxybenzoic acid butyl ester**	**-7.2**	**-7.2**	**-7.2**	**-7.2**	**-7.2**	**-7.20**	**0.0000**
6	**3,4-dihydroxybenzoic acid ethyl ester**	**-6**	**-5.9**	**-6**	**-6.2**	**-6.1**	**-6.04**	**0.1140**
7	**3,4-dihydroxybenzoic acid methyl ester**	**-6**	**-5.9**	**-6**	**-6**	**-6**	**-5.98**	**0.0447**
8	**4-Caffeoylquinic acid**	**-8.8**	**-8.8**	**-8.8**	**-8.8**	**-8.8**	**-8.80**	**0.0000**
9	**4-Methoxycinnamic acid**	**-6.1**	**-6**	**-6**	**-5.8**	**-6**	**-5.98**	**0.1095**
10	**5-Methoxysalicylic Acid**	**-6.1**	**-6.1**	**-6.1**	**-6.1**	**-6.1**	**-6.10**	**0.0000**
11	**Caffeic acid**	**-6.2**	**-6.2**	**-6.3**	**-6.2**	**-6.2**	**-6.22**	**0.0447**
12	**Chlorogenic acid**	**-8.2**	**-8.2**	**-8.2**	**-8.2**	**-8.2**	**-8.20**	**0.0000**

13	Cinnamic acid	-5.9	-5.9	-5.8	-5.9	-5.8	-5.86	0.0548
14	D-3-Phenyllactic acid	-6	-6	-6.1	-6	-6	-6.02	0.0447
15	Ellagic acid	-9.7	-9.7	-9.7	-9.7	-9.7	-9.70	0.0000
16	Ethyl gallate	-6	-6.1	-6.1	-6.1	-6.1	-6.08	0.0447
17	Ferulic acid	-6.2	-6.2	-6.2	-6.2	-6.2	-6.20	0.0000
18	Gallic acid	-6.3	-6.3	-6.3	-6.3	-6.3	-6.30	0.0000
19	Gallic acid ethyl ester	-6.1	-6.0	-6.0	-6.0	-6.0	-6.02	0.0447
20	Gentisic acid	-6.0	-6.0	-6.0	-6.0	-6.0	-6.00	0.0000
21	Hydroxybenzoic acid	-5.7	-5.7	-5.7	-5.7	-5.7	-5.70	0.0000
22	Isovanillic acid	-6.3	-6.3	-6.3	-6.3	-6.3	-6.30	0.0000
23	m-Coumaric acid	-6.2	-6.3	-6.3	-6.3	-6.3	-6.28	0.0447
24	Methyl ferulate	-6.0	-6.1	-6.1	-6.1	-6.1	-6.08	0.0447
25	Methyl gallate	-6.2	-6.2	-6.2	-6.2	-6.2	-6.20	0.0000
26	o-Coumaric acid	-6.2	-6.2	-6.2	-6.2	-6.2	-6.20	0.0000
27	p-Coumaric acid	-6.5	-6.5	-6.5	-6.5	-6.5	-6.50	0.0000
28	p-Coumaric acid-O-glucoside	-7.8	-7.8	-7.8	-7.8	-7.8	-7.80	0.0000
29	Protocatechuic acid	-6.1	-6.1	-6.1	-6.1	-6.1	-6.10	0.0000
30	Protocatechuic acid methyl ester	-6	-6	-6	-6	-6	-6.00	0.0000
31	Rosmarinic acid	-7.8	-7.6	-7.6	-8.5	-8	-7.90	0.3742
32	Salicylic acid	-5.7	-5.7	-5.7	-5.7	-5.7	-5.70	0.0000
33	Sinapic acid	-6.3	-6.4	-6.3	-6.4	-6.3	-6.34	0.0548
34	Syringic acid	-5.7	-5.7	-5.7	-5.7	-5.9	-5.74	0.0894
35	trans-Cinnamate	-5.8	-5.8	-5.8	-5.8	-5.8	-5.80	0.0000
36	trans-Methyl p-coumarate	-6.1	-6.1	-6.1	-6.1	-6.1	-6.10	0.0000
37	Vanillic acid	-6.1	-5.9	-5.9	-6.0	-5.9	-5.96	0.0894
Overall Mean								0.0461

Protein and Ligand Library

Table 1. Selected human receptor proteins with PDB ID, method, and resolution.

Sl No	Receptor	PDB ID	Organism	Method	Resolution
1	NagZ–GlcNAc (Ng)	6JTJ	Neisseria gonorrhoeae	X-RAY DIFFRACTION	2.18 Å

Table 2. Selected Ligands with PubChem ID and SMILES.

SI No	Phytochemicals	PubChem ID	SMILES
1	**1-O-sinapoyl-beta-D-glucose**	5280406	COC1=CC(=CC(=C1O)OC)/C=C/C(=O)O[C@H]2[C@@H]([C@H]([C@@H]([C@H](O2)CO)O)O)O
2	**3-Hydroxybenzoic acid**	7420	C1=CC(=CC(=C1)O)C(=O)O
3	**3,4-di-O-caffeoylquinic acid**	5281780	C1[C@H]([C@H]([C@@H](C[C@@]1(C(=O)O)O)OC(=O)/C=C/C2=CC(=C(C=C2)O)O)OC(=O)/C=C/C3=CC(=C(C=C3)O)O)O
4	**3,4-dihydroxy-trans-cinnamic acid or**	1549111	C1=CC(=C(C=C1/C=C\C(=O)O)O)O
5	**3,4-dihydroxybenzoic acid butyl ester**	528594	CC(C)(C)[Si](C)(C)OC1=C(C=C(C=C1)C(=O)O[Si](C)(C)C(C)(C)C)O[Si](C)(C)C(C)(C)C
6	**3,4-dihydroxybenzoic acid ethyl ester**	77547	CCOC(=O)C1=CC(=C(C=C1)O)O
7	**3,4-dihydroxybenzoic acid methyl ester**	287064	COC(=O)C1=CC(=C(C=C1)O)O

ISSN No. 2321-2705 | DOI: 10.51244/IJRSI |Volume XIII Issue VI June 2026

8	**4-Caffeoylquinic acid**	9798666	C1[C@H](C([C@@H](CC1(C(=O)O)O)O)OC(=O)/C=C/C2=CC(=C(C=C2)O)O)O
9	**4-Methoxycinnamic acid**	699414	COC1=CC=C(C=C1)/C=C/C(=O)O
10	**5-Methoxysalicylic acid**	75787	COC1=CC(=C(C=C1)O)C(=O)O
11	**Caffeic acid**	689043	C1=CC(=C(C=C1/C=C/C(=O)O)O)O
12	**Chlorogenic acid**	1794427	C1[C@H]([C@H]([C@@H](C[C@@]1(C(=O)O)O)OC(=O)/C=C/C2=CC(=C(C=C2)O)O)O)O
13	**Cinnamic acid**	444539	C1=CC=C(C=C1)/C=C/C(=O)O
14	**D-3-Phenyllactic acid**	643327	C1=CC=C(C=C1)C[C@H](C(=O)O)O
15	**Ellagic acid**	5281855	C1=C2C3=C(C(=C1O)O)OC(=O)C4=CC(=C(C(=C43)OC2=O)O)O
16	**Ethyl gallate**	13250	CCOC(=O)C1=CC(=C(C(=C1)O)O)O
17	**Ferulic acid**	445858	COC1=C(C=CC(=C1)/C=C/C(=O)O)O
18	**Gallic acid**	370	C1=C(C=C(C(=C1O)O)O)C(=O)O
19	**Gallic acid ethyl ester**	14250	CCOC(=O)C1=CC(=C(C(=C1)O)O)O
20	**Gentisic acid**	3469	C1=CC(=C(C=C1O)C(=O)O)O
21	**Hydroxybenzoic acid**	135	C1=CC(=CC=C1C(=O)O)O
22	**Isovanillic acid**	12575	COC1=C(C=C(C=C1)C(=O)O)O
23	**m-Coumaric acid**	637541	C1=CC(=CC(=C1)O)/C=C/C(=O)O
24	**Methyl ferulate**	5357283	COC1=C(C=CC(=C1)/C=C/C(=O)OC)O
25	**Methyl gallate**	7428	COC(=O)C1=CC(=C(C(=C1)O)O)O
26	**o-Coumaric acid**	637540	C1=CC=C(C(=C1)/C=C/C(=O)O)O
27	**p-Coumaric acid**	637542	C1=CC(=CC=C1/C=C/C(=O)O)O
28	**p-Coumaric acid-O-glucoside**	9840292	C1=CC(=CC=C1/C=C/C(=O)O)O[C@H]2[C@@H]([C@H]([C@@H]([C@H](O2)CO)O)O)O
29	**Protocatechuic acid**	72	C1=CC(=C(C=C1C(=O)O)O)O
30	**Protocatechuic acid methyl ester**	287064	COC(=O)C1=CC(=C(C=C1)O)O
31	**Rosmarinic acid**	5281792	C1=CC(=C(C=C1C[C@H](C(=O)O)OC(=O)/C=C/C2=CC(=C(C=C2)O)O)O)O
32	**Salicylic acid**	338	C1=CC=C(C(=C1)C(=O)O)O
33	**Sinapic acid**	10743	COC1=CC(=CC(=C1O)OC)C=CC(=O)O
34	**Syringic acid**	10742	COC1=CC(=CC(=C1O)OC)C(=O)O
35	**trans-Cinnamate**	5957728	C1=CC=C(C=C1)/C=C/C(=O)[O-]
36	**trans-Methyl p-coumarate**	5319562	COC(=O)/C=C/C1=CC=C(C=C1)O
37	**Vanillic acid**	8468	COC1=C(C=CC(=C1)C(=O)O)O

Table 3. Phenolic Acids and their Plant Sources

Plant Name	Family	Common Name	IDENTIFIED PHENOLIC ACIDS	Cid Number	REFERENCES
Abrus precatorius	Fabaceae (Subfamily: Faboideae)	rosary pea or jequirity bean	Gallic acid Vanillic acid Syringic acid Caffeic acid p-Coumaric acid Ferulic acid	370 8468 10742 689043 637542 445858	https://journals.innovareacademics.in/index.php/ijpps/article/view/6435/6878 https://doi.org/10.1080/14786419.2017.1378217
Acacia confusa	Fabaceae (Subfamily: Caesalpinioideae)	small Philippine acacia and F	3,4-dihydroxybenzoic acid methyl ester 3,4-dihydroxybenzoic acid ethyl ester 3,4-dihydroxybenzoic acid butyl ester 3,4-dihydroxy-trans-cinnamic acid	287064 77547 528594 1549111	https://doi.org/10.1016/j.biortech.2006.04.017

		ormosa acacia	gallic acid gallic acid ethyl ester	370 14250	https://doi.org/10.1016/j.jtcme.2018.05.002
Acacia auriculiformis	Fabaceae (Subfamily: Mimosoideae)	ear-pod wattle	Protocatechuic acid	72	https://doi.org/10.1021/jf050550m
Acacia mangium	Fabaceae (Subfamily: Caesalpinioideae)	brown salwood	Ferulic acid	445858	https://doi.org/10.31686/ijier.vol8.iss12.2860
Acaciella angustissima	Fabaceae (Subfamily: Mimosoideae)	Timbe, Prairie Acacia, or White-Ball Acacia	Gallic acid Protocatechuic acid	370 72	https://doi.org/10.29169/1927-5951.2020.10.06.2
Albizia lebbeck	Fabaceae (Subfamily: Mimosoideae)	Siris tree	Gallic acid m-Coumaric acid Sinapic acid	370 637541 10743	https://doi.org/10.3390/medicina55050184
Archidendron paucifloru m	Fabaceae (Subfamily: Mimosoideae)	jengkol or djenko	Gallic acid p-Coumaric acid	370 637542	https://doi.org/10.1016/j.bcab.2021.102039
Adenanthera pavonina	Fabaceae (Subfamily: Mimosoideae	Red Bead Tree, Coral Wood, or Saga Tree	Gallic acid Caffeic acid Chlorogenic acid p-Coumaric acid Sinapic acid	370 689043 1794427 637542 10743	https://doi.org/10.3390/plants12223902
Arachis hypogaea	Fabaceae (Subfamily: Faboideae)	Peanut	Gallic acid Protocatechuic acid Caffeic acid p-Coumaric acid Chlorogenic acid Syringic acid Vanillic acid Ferulic acid Rosmarinic acid	370 72 689043 637542 1794427 10742 8468 445858 5281792	https://doi.org/10.1007/s11947-022-02901-5
Bauhinia acuminata	Fabaceae (Subfamily: Cercidoideae)	dwarf white orchid tree	Gallic acid Vanillic acid p-Coumaric acid	370 8468 637542	https://doi.org/10.1016/j.jaim.2025.101127
Bauhinia variegata	Fabaceae (Subfamily: Cercidoideae)	Mountain ebony	Protocatechuic acid	72	https://doi.org/10.3390/antiox8100492
Biancaea sappan	Fabaceae (Subfamily: Caesalpinioideae)	sappanwood	Gallic acid Caffeic acid Chlorogenic acid	370 689043 1794427	https://doi.org/10.3390/molecules28176247
Caesalpinia pulcherrima	Fabaceae (Subfamily: Caesalpinioideae)	Peacock Flower or Pride of Barbados	Gallic acid Ellagic acid	370 5281855	https://doi.org/10.4103/pm.pm_100_19

Cajanus cajan	Fabaceae (Subfamily: Faboideae)	Pigeon pea	Gallic acid Protocatechuic acid Vanillic acid Caffeic acid p-Coumaric acid Ferulic acid Chlorogenic acid Syringic acid	370 72 8468 689043 637542 445858 1794427 10742	https://doi.org/10.15835/nbha52313674
Cajanus scarabaeoides	Fabaceae (Subfamily: Faboideae)	Showy Pigeonpea	Gallic acid Caffeic acid Ferulic acid	370 689043 445858	https://doi.org/10.1371/journal.pone.0208201
Cassia javanica	Fabaceae (Subfamily: Caesalpinioideae)	Java cassia or pink shower tree	Gallic acid Chlorogenic acid Syringic acid Ferulic acid Vanillic acid o-Coumaric acid Cinnamic acid	370 1794427 10742 445858 8468 637540 444539	https://doi.org/10.3390/molecules27144329
Canavalia ensiformis	Fabaceae (Subfamily: Faboideae)	Jack bean	Gallic acid	370	https://doi.org/10.24167/jfcn.v1i2.12751
Clitoria ternatea	Fabaceae (Subfamily: Faboideae)	butterfly pea or Asian pigeonwings	Gallic acid Caffeic acid Ferulic acid p-Coumaric acid Chlorogenic acid Ellagic acid Cinnamic acid	370 689043 445858 637542 1794427 5281855 444539	https://doi.org/10.3390/app13042134
Crotalaria juncea	Fabaceae (Subfamily: Faboideae)	Sunn Hemp	Gallic acid	370	https://doi.org/10.5114/bta.2023.132772
Cassia fistula	Fabaceae (Subfamily: Caesalpinioideae)	Golden Shower tree	Gallic acid Caffeic acid Ferulic acid Vanillic acid Syringic acid p-Coumaric acid Ellagic acid 3,4-di-O-caffeoylquinic acid 4-Methoxycinnamic acid	370 689043 445858 8468 10742 637542 5281855 5281780 699414	https://doi.org/10.1016/j.heliyon.2022.e10251
Cassia grandis	Fabaceae (Subfamily: Caesalpinioideae)	Pink Shower Tree or Horse Cassia	Gallic acid Caffeic acid Ferulic acid Vanillic acid Syringic acid p-Coumaric acid Ellagic acid	370 689043 445858 8468 10742 637542 5281855	https://doi.org/10.3390/molecules27175590
Dalbergia sissoo	Fabaceae (Subfamily: Faboideae)	Indian Rosewood or Shisham	5-Methoxysalicylic acid Caffeic acid Chlorogenic acid trans-Cinnamate Gallic acid	75787 689043 1794427 5957728 370	https://doi.org/10.21608/aijpms.2023.190847.1190 Sharh https://doi.org/10.54085/ap.2022.11.1.43

Delonix regia	Fabaceae (Subfamily: Caesalpinioideae)	Royal Poinciana or Flamboyant tree	Gallic acid Protocatechuic acid Chlorogenic acid Sinapic acid p-Coumaric acid m-Coumaric acid Ferulic acid Caffeic acid	370 72 1794427 10743 637542 637541 445858 689043	https://doi.org/10.3390/molecules16097302
Entada phaseoloides	Fabaceae (Subfamily: Mimosoideae)	St. Thomas Bean	Protocatechuic acid	72	https://doi.org/10.3390/molecules27020440
Entada rheedei	Fabaceae (Subfamily: Caesalpinioideae)	African dream herb or giant sea bean	Protocatechuic acid Protocatechuic acid methyl ester	72 287064	https://doi.org/10.7324/japs.2018.8513
Erythrina variegata	Fabaceae (Subfamily: Faboideae)	Indian coral tree or tiger's claw	Gallic acid Caffeic acid	370 689043	https://doi.org/10.1016/j.jams.2016.06.001
Gliricidia sepium	Fabaceae (Subfamily: Faboideae)	Madre de Cacao or Ka kawate	p-Coumaric acid Ferulic acid Caffeic acid	637542 445858 689043	https://doi.org/10.1016/j.matdes.2024.112130
Glycine tomentella	Fabaceae (Subfamily: Faboideae)	Rusty Glycine or Woolly Glycine	Ferulic acid Caffeic acid	445858 689043	https://doi:10.1016/j.foodchem.2010.01.004
Glycine max	Fabaceae (Subfamily: Faboideae)	soybean	p-Coumaric acid Ferulic acid Caffeic acid	637542 445858 689043	https://doi.org/10.1016/j.jfca.2022.104717 https://doi.org/10.1007/s00217-005-0153-4 https://doi.org/10.1002/fft2.376
Haematoxylum campechianum	Fabaceae (Subfamily: Caesalpinioideae)	Logwood	Gallic acid Methyl gallate Ethyl gallate	370 7428 13250	https//:doi.org.10.1016/S0031-9422(98)00667-0
Hymenaea courbaril	Fabaceae (Subfamily: Caesalpinioideae)	West Indian Locust	Gallic acid p-Coumaric acid Ferulic acid	370 637542 445858	https://doi.org/10.1016/j.indcrop.2013.06.005 https://doi.org/10.1002/cbdv.202503154
Inga edulis	Fabaceae (Subfamily: Caesalpinioideae)	ice-cream bean	Gallic acid Chlorogenic acid Caffeic acid	370 1794427 689043	https://doi.org/10.3390/agriculture14122337
Indigofera linifolia	Fabaceae (Subfamily: Faboideae)	narrowleaf indigo	Caffeic acid Hydroxybenzoic acid Syringic acid Chlorogenic acid	689043 135 10742 1794427	https://doi.org/10.3390/molecules27154707

Lablab purpureus	Fabaceae (Subfamily: Faboideae)	Hyacinth bean	Ferulic acid p-Coumaric acid Caffeic acid	445858 637542 689043	https://doi.org/10.1186/s43014-024-00289-7
Lespedeza cuneata	Fabaceae (Subfamily: Faboideae)	sericea lespedeza or Chinese bushclover	Gallic acid Caffeic acid Ferulic acid	370 689043 445858	https://doi.org/10.3390/molecules30092013
Leucaena leucocephala	Fabaceae (Subfamily: **Mimosoideae**)	White leadtree	Gallic acid Ferulic acid	370 445858	https://doi.org/10.1007/s13399-022-03420-1 https://doi.org/10.3390/plants11131672
Macrotyloma uniflorum	Fabaceae (Subfamily: Faboideae)	Horse gram	p-coumaric acid Gallic acid Protocatechuic acid Vanillic acid Syringic acid Caffeic acid Chlorogenic acid Ferullic acid Sinapic acid	637542 370 72 8468 10742 689043 1794427 445858 10743	https://doi.org/10.1007/s13197-014-1312-z
Medicago lupulina	Fabaceae (Subfamily: Faboideae)	Black medick	Caffeic acid Ferulic acid	689043 445858	https://doi.org/10.3390/molecules26061610
Medicago polymorpha	Fabaceae (Subfamily: Faboideae)	Burclover or California burclover	sinapic acid 4-caffeoylquinic acid rosmarinic acid caffeic acid	10743 9798666 5281792 689043	https://doi.org/10.1016/j.ejmcr.2024.100164
Melilotus indicus	Fabaceae (Subfamily: Faboideae)	Indian sweet-clover	Vanillic acid, O-coumaric acid m-coumaric acid P-coumaric acid-O-Glucoside Ferulic acid Chlorogenic acid Gallic acid Caffeic acid Syringic acid	8468 637540 637541 9840292 445858 1794427 370 689043 10742	https://doi.org/10.1021/acsomega.2c03053
Mezoneuron pubescens	Fabaceae (Subfamily: Caesalpinioideae)	Cat's Claw Liana	Gallic acid	370	https://doi.org/10.55463/issn.1674-2974.49.2.15
Mimosa pudica	Fabaceae (Subfamily: Caesalpinioideae)	sensitive plant	p-coumaric acid Protocatechuic acid Caffeic acid Ferulic acid Cinnamic acid Chlorogenic acid Gallic acid	637542 72 689043 445858 444539 1794427 370	https://doi.org/10.1016/j.prmcm.2023.100241
Mucuna pruriens	Fabaceae (Subfamily: Faboideae)	Velvet bean	gallic acid caffeic acid chlorogenic acid ferulic acid p-coumaric acid	370 689043 1794427 445858 637542	https://doi.org/10.1016/j.focha.2023.100503

Neptunia oleracea	Fabaceae (Subfamily: Mimosoideae)	Water Mimosa	Gallic acid Caffeic acid Ferulic acid	370 689043 445858	https://doi.org/10.1016/j.phytol.2016.02.014
Ototropis sequax	Fabaceae (Subfamily: Faboideae)	Sinuate-leaf tickclover	Chlorogenic acid	1794427	https://www.researchgate.net/publication/268262246_Antioxidant_activities_of_phenolic_components_from_various_plants_of_Desmodium_species#:~:text=fingerprints%20were%20established%2C%20and%20chl,ioxidant%20activity%20of%20this%20plant.
Pachyrhizus erosus	Fabaceae (Subfamily: Faboideae)	Jicama	Caffeic acid Ferulic acid Chlorogenic acid protocatechuic acid Vanillic acid	689043 445858 1794427 72 8468	https://doi.org/10.3390/cosmetics10060164
Parkia speciosa	Fabaceae (Subfamily: Mimosoideae)	Stink bean	Gallic acid Chlorogenic acid ellagic acid vanillic acid caffeic acid	370 1794427 5281855 8468 689043	https://doi.org/10.1080/10942912.2013.775152
Parkia timoriana	Fabaceae (Subfamily: Mimosoideae)	Tree bean	Gallic acid Chlorogenic acid	370 1794427	https://doi.org/10.3389/fsufs.2025.1628357
Peltophorum pterocarpum	Fabaceae (Subfamily: Caesalpinioideae)	Copperpod or yellow flame tree	Isovanillic acid methyl ferulate vanillic acid syringic acid	12575 5357283 8468 10742	https://doi.org/10.3390/molecules24020240
Phanera semibifida	Fabaceae (Subfamily: Cercidoideae)	Silver underside	Salicylic acid	338	https://doi.org/10.13057/biodiv/d260149
Phaseolus lunatus	Fabaceae (Subfamily: Faboideae)	Lima bean	p-Coumaric acid caffeic acid ferulic acid gallic acid	637542 689043 445858 370	https://doi.org/10.7455/ijfs/8.1.2019.a9
Phaseolus vulgaris	Fabaceae (Subfamily: Faboideae)	Bean	p-Coumaric acid caffeic acid ferulic acid vanillic acid	637542 689043 445858 8468	https://doi.org/10.1021/jf051706l
Phyllodium pulchellum	Fabaceae (Subfamily: Faboideae)	Showy Desmodium	Protocatechuic acid p-Coumaric acid	72 637542	https://doi.org/10.3390/molecules23061361
Pithecellobium dulce	Fabaceae (Subfamily: **Caesalpinioideae**)	Manila tamarind or kamachile	Gallic acid Ferulic acid	370 445858	https://doi.org/10.1038/s41598-025-32257-7
Pleurolobus gangeticus	Fabaceae (Subfamily: Papilionoideae)	Salparni	Caffeic acid Salicylic acid	689043 338	https://doi.org/10.1007/s44372-024-00068-1

Pongamia pinnata	Fabaceae (Subfamily: Faboideae)	Indian beech tree	Protocatechiuc acid Ellagic acid Ferulic acid Gallic acid Gentisic acid p-coumaric acid Salicylic acid	72 5281855 445858 370 3469 637542 338	https://doi.org/10.3390/molecules17043917
Prosopis juliflora	Fabaceae (Subfamily: **Caesalpinioideae**)	Mesquite	Gallic acid Ferulic acid Caffeic acid p-coumaric acid	370 445858 689043 637542	https://doi.org/10.3390/biom9120777
Pseudatharia viscida	Fabaceae (Subfamily: Faboideae)	Moovilai	Gallic acid Ferulic acid Caffeic acid	370 445858 689043	https://doi.org/10.21474/ijar01
Psophocarpus tetragonolobus	Fabaceae (Subfamily: Papilionoideae)	winged bean	Gallic acid	370	https://doi.org/10.3390/biology14121646
Pterocarpus indicus	Fabaceae (Subfamily: Faboideae)	Brumese-Rosewood	Caffeic acid ferulic acid p-Coumaric acid	689043 445858 637542	https://doi.org/10.1177/1559325825141404
Pterocarpus marsupium	Fabaceae (Subfamily: Faboideae)	Indian kino tree or Malabar kino	Caffeic acid ferulic acid p-Coumaric acid	689043 445858 637542	https://doi.org/10.3390/plants11030247
Pueraria montana	Fabaceae (Subfamily: Faboideae)	kudzu	Caffeic acid ferulic acid	689043 445858	https://doi.org/10.3389/fnut.2022.868188
Pueraria lobata	Fabaceae (Subfamily: Faboideae)	Ge-Gen	Caffeic acid ferulic acid	689043 445858	https://doi.org/10.3389/fnut.2022.868188
Pueraria thomsonii	Fabaceae (Subfamily: Faboideae)	Starch kudzu	Caffeic acid ferulic acid	689043 445858	https://doi.org/10.3389/fnut.2022.868188
Rhynchosia minima	Fabaceae (Subfamily: Faboideae)	least snout-bean	Gallic acid	370	https://doi.org/10.5958/0974-360X.2020.00334.0
Samanea saman	Fabaceae (Subfamily: **Caesalpinioideae**)	Rain tree	Gallic acid Caffeic acid	370 689043	https://doi.org/10.24843/JCHEM.v12,i02.p05
Saraca indica	Fabaceae (Subfamily: Detarioideae)	Ashoka tree	Protocatechuic acid Chlorogenic acid Caffeic acid p-coumaric acid Ferulic acid Cinnamic acid Gallic acid Vanillic	72 1794427 689043 637542 445858 444539 370 8468	https://doi.org/10.1186/s43094-022-00430-8

Saraca thaipingensis	Fabaceae (Subfamily: Detarioideae)	Yellow Saraca	p-coumaric acid	637542	https://doi.org/10.1186/s43094-022-00430-8
Senegalia catechu	Fabaceae (Subfamily: Caesalpinioideae)	black cutch or cutch tree	Gallic acid Ellagic acid	370 5281855	https://doi.org/10.22271/phyto.2023.v12.i6b.14779
Senna alata	Fabaceae (Subfamily: **Caesalpinioideae**)	candle bush	Gallic acid p-Coumaric acid ferulic acid	370 637542 445858	https://www.irejournals.com/paper-details/1703474
Senna occidentalis	Fabaceae (Subfamily: **Caesalpinioideae**)	Coffee senna	Gallic acid Ferulic acid	370 445858	https://doi.org/10.1002/fsn3.4705
Senna siamea	Fabaceae (Subfamily: **Caesalpinioideae**)	Siamese Senna	Gallic acid Ferulic acid	370 445858	https://doi.org/10.1016/j.toxrep.2024.101793
Sesbania grandiflora	Fabaceae (Subfamily: Faboideae)	vegetable hummingbird	Caffeic acid Ferulic acid	689043 445858	https://doi.org/10.3390/ph18010064
Sesbania sesban	Fabaceae (Subfamily: Faboideae)	Sesban	Ferulic acid Caffeic acid	445858 689043	https://doi.org/10.3390/ph18010064
Sophora tomentosa	Fabaceae (Subfamily: Faboideae)	necklacepod	Ferulic acid Caffeic acid	445858 689043	https://doi.org/10.3390/nu11020252
Stylosanthes guianensis	Fabaceae (Subfamily: Faboideae)	stylo	Ferulic acid Caffeic acid p-Coumaric acid	445858 689043 637542	https://doi.org/10.5539/jas.v12n11p209
Tamarindus indica	Fabaceae (Subfamily: Detarioideae)	Tamarind	Ferulic acid Caffeic acid	445858 689043	https://doi.org/10.1039/D4FO03595J
Tephrosia purpurea	Fabaceae (Subfamily: Faboideae)	Purple hoarypea	Gallic acid Ferulic acid Chlorogenic acid Caffeic acid p-coumaric acid	370 445858 1794427 689043 637542	https://doi.org/10.3390/molecules28093939
Trifolium repens	Fabaceae (Subfamily: Faboideae)	White clover	Ferulic acid Caffeic acid p-Coumaric acid	445858 689043 637542	https://doi.org/10.1007/s13205-020-02539-0
Uraria crinita	Fabaceae (Subfamily: Faboideae)	Asian Foxtail	salicylic acid	338	https://doi.org/10.1039/d0fo00782j
Uraria picta	Fabaceae (Subfamily: Faboideae)	Prishniparni	Gallic acid	370	http://dx.doi.org/10.13005/bbra/2937

ISSN No. 2321-2705 | DOI: 10.51244/IJRSI |Volume XIII Issue VI June 2026

Vachellia farnesiana	Fabaceae (Subfamily: Caesalpinioideae)	sweet acacia	Gallic acid	370	https://doi.org/10.1016/j.prenap.2025.100245
Vigna mungo	Fabaceae (Subfamily: Faboideae)	Black gram	Gallic acid Protocatechuic acid Gentisic acid Vanillic acid Syringic acid Caffeic acid Ferulic acid	370 72 3469 8468 10742 689043 445858	https://doi.org/10.1016/j.foodres.2011.12.026
Vigna radiata	Fabaceae (Subfamily: Faboideae)	Mung bean	Syringic acid Vanillic acid Isovanillic acid Protocatechuic acid Gentisic acid Gallic acid Chlorogenic acid p-coumaric acid caffeic acid cinnamic acid sinapic acid	10742 8468 12575 72 3469 370 1794427 637542 689043 444539 10743	https://doi.org/10.1002/leg3.70
Vigna subterranea (L.)	Fabaceae (Subfamily: Faboideae)	Bambara groundnut	p-coumaric acid caffeic acid ferulic acid	637542 689043 445858	https://doi.org/10.3390/molecules27165265
Vigna umbellata	Fabaceae (Subfamily: Faboideae)	Rice bean	Gallic acid Protocatechuic acid Syringic acid Ellagic acid Caffeic acid p-coumaric acid Sinapic acid Ferulic acid	370 72 10742 5281855 689043 637542 10743 445858	https://doi.org/10.3390/foods12142718
Vigna angularis	Fabaceae (Subfamily: Faboideae)	adzuki bean or red bean	Chlorogenic acid Gallic acid Ferulic acid Syringic acid Caffeic acid	1794427 370 445858 10742 689043	https://doi.org/10.3390/molecules27186079
Zapoteca portoricensis	Fabaceae (Subfamily: Caesalpinioideae)	white stickpea	Gallic acid	370	https://unicrossjournals.com/images/document/15599052/12-jmr8R17ZwyfPjoki5N4xdA.pdf